UNIVERSITY OF TURKU

CRISPR/Cas9-mediated knockout of *mmp13a*, *mmp13b*, *slc5a1*, and *slc5a2* in a hypoxia-induced zebrafish embryo heart failure model

MDP in Drug Discovery and Development, Institute of Biomedicine
Master's thesis

Author:
Sk Jahid Hasan

Supervisor:
PhD, Doc. Ilkka Paatero; Turku Bioscience Centre, University of Turku and Åbo Akademi University

30.04.2026
Turku

I hereby declare that generative artificial intelligence was used as a supportive tool in the preparation of this thesis. The work remains entirely my own, and I am fully responsible for all content. Details of the tools used, and their specific applications are provided in Appendix A

The originality of this thesis has been checked in accordance with the University of Turku quality assurance system using the Turnitin Originality Check service.

Master's thesis

Subject: Institute of Biomedicine, MDP in Drug Discovery and Development

Author: Sk Jahid Hasan

Title: CRISPR/Cas9-mediated knockout of *mmp13a*, *mmp13b*, *slc5a1*, and *slc5a2* in a hypoxia-induced zebrafish embryo heart failure model

Supervisors: PhD, Doc. Ilkka Paatero, Turku Bioscience Centre, University of Turku and Åbo Akademi University

Number of pages: 94 pages
Date: 30.04.2026

Heart failure (HF) is a complex condition where the heart is unable to provide sufficient blood supply to meet the metabolic need. Myocardial infarction (MI) is the major cause for developing heart failure, and the prevalence of heart failure is over 10% in individuals over the age of 70. The zebrafish (*Danio rerio*) is widely used as an animal model for cardiovascular diseases, including heart failure. The highly conserved hypoxia response in vertebrates makes zebrafish a suitable disease model to study heart failure. In this study, I aimed to evaluate the role of *the mmp13a, mmp13b*, *slc5a1*, and *slc5a2* genes in heart failure in a hypoxia-induced zebrafish embryo heart failure model using CRISPR/Cas9-mediated gene knockout techniques. The target genes were knocked out by microinjecting the Cas9 ribonucleoprotein (RNP) complex into the early-stage zebrafish embryos. The embryos were exposed to hypoxia at three days post-fertilization (3 dpf), and the heart was imaged at 4 dpf. The diameter of the heart at diastole and systole was measured, and the fractional shortening (FS%) was calculated. There was no difference in FS% after gene knockout without hypoxia exposure. After 45 minutes of hypoxia exposure, a reduction in the FS% was observed in the *mmp13b* knockout group, and after 60 minutes of hypoxia exposure, an improvement in the FS% was observed in the *slc5a1* and *slc5a2* knockout groups. These results suggest that knockout of *slc5a1* and *slc5a2* improves cardiac function (FS%), while *mmp13b* knockout impairs it under hypoxia-induced heart failure conditions in zebrafish embryos.

Keywords: Heart failure, CRISPR/Cas9, *mmp13a*, *mmp13b*, *slc5a1*, *slc5a2*, zebrafish

Table of Contents

1. Introduction

Heart failure

Heart failure (HF) can be defined as the heart's inability to provide sufficient blood supply to meet the metabolic need, and various conditions can lead to HF, such as ischemic heart disease and hypertension (Kemp & Conte, 2012). It is a complex condition that may result from functional or structural dysfunction, leading to decreased capacity of the ventricle to supply blood to different parts of the body (Warriner et al., 2015). When the heart is failing, the body tries to compensate through various mechanisms, which can be beneficial during the early stages but worsens HF in the long run. These may include an increase in cardiac output, myocardial remodeling, and different neurohormonal systems activation (Kemp & Conte, 2012). HF is not considered a dysfunction of a single organ; rather, it affects multiple organ systems in the body (Warriner et al., 2015).

Epidemiology

Approximately one third of all global deaths are caused by various cardiovascular diseases, making it the leading cause of mortality worldwide, accounting for 20.5 million deaths (Cesare et al., 2024). Annually, various cardiovascular diseases cause approximately 55% of deaths in women and 43% of deaths in men in Europe (Liu et al., 2024).

The prevalence of HF is increasing with the aging population, and worldwide it is currently affecting around 64 million people (Shahim et al., 2023). The overall prevalence of HF in Europe and the USA can range from 1-12%. In the adult population, it is estimated to be 1–2%, but in the population aged over 70, it can rise to over 10%. The lifetime risk of HF after age 55 is 33% and 28% for men and women, respectively (Ponikowski et al., 2016). The prevalence of heart failure is up to 22% in patients with diabetes (Pop-Busui et al., 2022). Currently, in Finland, the prevalence of heart failure is 13.9 per 1,000 individuals, with a five-year mortality rate of 62.6% among HF patients, and it is estimated that 16.7% of

people over age 65 seeking medical care for shortness of breath have undiagnosed heart failure. (Huusko et al., 2019).

Classification

Heart failure can be classified into three major categories based on the left ventricular ejection fraction (LVEF): HF with preserved ejection fraction (HFpEF), HF with mildly reduced ejection fraction (HFmrEF), and HF with reduced ejection fraction (HFrEF) (Table 1). HF with improved ejection fraction (HFimEF) is a new category that has been recently introduced, as the LVEF demonstrates an absolute increase of ≥10% to a value higher than 40% in 10% to 60% patients with HFrEF (Profire et al., 2025).

Older people, mostly older women with a previous history of hypertension and atrial fibrillation, are more often diagnosed with HFpEF rather than HFrEF. A mixture of HFpEF and HFrEF characteristics is observed in the patients with HFmrEF. This indicates that patients with HFmrEF may experience symptoms and clinical features that overlap between HFpEF and HFrEF, which complicates their diagnosis and treatment (Ponikowski et al., 2016).

Table 1. Heart failure classification and corresponding LVEF values

Category	**LVEF**	**EF Status**
HFpEF	≥ 50%	Preserved
HFmrEF	41-49%	Mildly reduced
HFrEF	≤ 40%	Reduced
HFimEF	>40% (+ ≥10% increase)	Improved

Etiology

Multiple factors are associated with the etiology of HF. For patient management and accurate diagnosis, understanding the underlying cause is necessary (Profire et al., 2025). Genetic predisposition plays a significant role in developing heart failure, and some genetic mutations can alter the cardiac structure, causing heart failure (Schwinger, 2021). Although there is no added diagnostic benefit of routine genetic testing in patients with a confirmed

clinical diagnosis of heart failure, in patients with hypertrophic cardiomyopathy or arrhythmogenic right ventricular cardiomyopathy, genetic counseling is still recommended (Ponikowski et al., 2016).

Two-thirds of HF cases can be linked to chronic conditions such as arterial hypertension and ischemic heart disease (Kozman et al., 2025). Changes in the structure of the heart can be observed in patients with prolonged high blood pressure, which can decrease the heart's ability to pump blood effectively (Ponikowski et al., 2016).

Ischemic heart disease is the leading cause for patients with HFrEF or HFmrEF. Hypertension and valvular diseases are more prevalent in those with HFpEF. The impact of these causes on prognosis differs by HF type. Ischemic etiology is linked to higher mortality in HFrEF, while hypertensive and valvular etiologies are more associated with hospital admissions in other HF groups (Schwinger, 2021). Valvular heart disease (VHD) can lead to heart failure through mechanical damage to the heart, and different valve damage is associated with different VHD-related heart failure phenotypes. Damages in different heart valves can impair the heart's ability to pump blood effectively, leading to increased oxygen demand and mitochondrial dysfunction. The progression of valvular heart disease is further promoted by valvular fibrosis caused by mitochondrial dysfunction (S. Zhang et al., 2023).

Myocarditis, an inflammatory disease of the heart muscle, can impair heart function and leads to heart failure. While various infectious and non-infectious factors can cause myocarditis, it is mostly caused by viral infections (Brociek et al., 2023). Although viral infections are the most common infectious factors for myocarditis, bacterial, fungal, and protozoal infections can also lead to myocarditis (Nappi, 2025).

In patients with diabetes, heart failure is the most common cardiovascular complication, and patients with diabetes can develop heart failure irrespective of the presence of hypertension or coronary heart disease (Pop-Busui et al., 2022).

Hypertension and ischemic heart disease are the main causes of heart failure in high-income countries. At the same time, valvular heart disease is becoming more common due

to an aging population. In low-income countries in Asia and Africa, the major concern is rheumatic heart disease. The similarity in heart failure patterns between middle-income and high-income countries is due to increased life expectancy, Western dietary habits, and environmental changes (McBeath & Cowie, 2022).

Pathophysiology

Heart failure's underlying mechanisms are complex and involve several factors. Inflammation, hypoxia, oxidative stress, and both genetic and environmental influences can trigger the migration of cardiac fibroblasts and their differentiation into myofibroblasts. This process leads to cardiac remodeling and diastolic dysfunction (Biegus et al., 2021; Parichatikanond et al., 2020). Conditions that cause chronic stress on the heart, such as hypertension, can lead to cardiac remodeling, which involves changes in the size and shape of the heart. These changes ultimately lead to impaired heart functions (Cohn et al., 2000).

Myocardial infarction (MI) is the most common cause for the development of heart failure, and acute myocardial infarction (AMI) can worsen HF through cardiac remodeling and other mechanical dysfunctions (Jugdutt, 2012). Chronic coronary artery disease (CAD) and AMI can lead to severe myocardial ischemia, where the metabolic need for oxygen is not met due to either reduced coronary blood supply or increased need for oxygen in the myocardium. Although hypoxia is playing a crucial role, the ischemic heart undergoes increased oxidative stress after reperfusion as the heart attempts to return to aerobic respiration and produces reactive oxygen species (ROS) that could be toxic to the myocardium. Compromised mitochondrial function during hypoxia causes this production of toxic levels of ROS (Shohet & Garcia, 2007). Oxidative stress causes endothelial dysfunction, leading to increased vascular resistance and cardiac demand. Endothelial dysfunction is involved in the pathophysiology of both heart failure with preserved ejection fraction (HFpEF) and heart failure with reduced ejection fraction (HFrEF) (Zuchi et al., 2020). People with heart failure often have higher levels of inflammatory markers, such as TNF-α, E-selectin, interleukin-6 (IL-6), and intercellular adhesion molecule 1 (ICAM-1).

Inflammaging, a chronic, low-level inflammation seen in older adults, is characterized by increased levels of TNF-α, IL-6, and interleukin-1 beta (IL-1β) compared to younger people. These inflammatory markers can then increase oxidative stress by activating nicotinamide adenine dinucleotide phosphate oxidase (NADPH oxidase, NOX) (Murphy et al., 2020). Moreover, CD4+ T lymphocytes and M1 macrophages can worsen the inflammatory response. At the same time, a decrease in the activity of anti-inflammatory regulatory T cells can increase the inflammatory response (H. Liu et al., 2024b). The sympathetic nervous system (SNS) and the renin-angiotensin-aldosterone system (RAAS) can cause neurohormonal activation (Figure 1). Activation of this process helps to maintain cardiac output, but prolonged activation becomes harmful as angiotensin II (Ang II) stimulates cardiomyocyte hypertrophy and interstitial fibrosis (McBeath & Cowie, 2022).

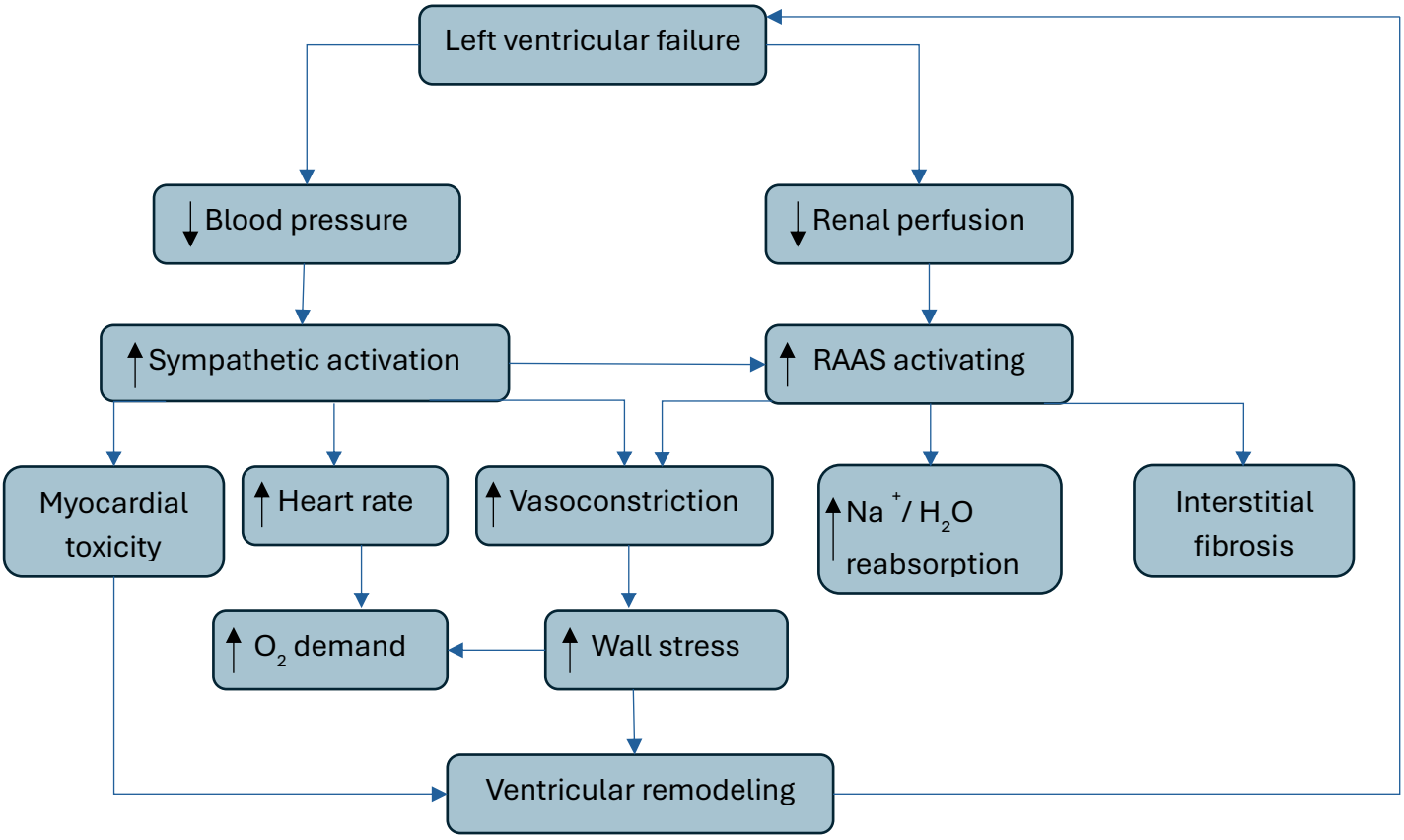

Figure 1. *The basic pathophysiology of heart failure due to left ventricular damage. Adopted from (McBeath & Cowie, 2022).*

Fractional shortening (FS%) is the change in diameter in the left ventricle (LV) during diastole and systole, and it is a rapid process that is often performed in emergency situations and can reflect how the left ventricle is operating (Weekes et al., 2012). Although FS% and ejection fraction (EF) are being used for the assessment of LV performance, in some cases, for example, in left ventricular hypertrophy (LVH), these two measurements can remain preserved, and mid-wall FS could be an alternative to conventional FS measurement to obtain more accurate insights (Yoshikawa et al., 2012).

Diagnosis of heart failure

The diagnosis of heart failure relies on the comprehensive assessment of clinical symptoms such as shortness of breath, persistent cough, fatigue, and generalized or lower extremity edema, as well as on various imaging techniques and biomarkers (Golla et al., 2026).

Echocardiography is a widely used, non-invasive imaging technique for the clinical diagnosis of heart failure. This technique can detect abnormalities in the heart valves and structural changes in heart failure. Heart failure can be categorized based on the echocardiographic assessment of the ejection fraction (EF) (Dini et al., 2024). Cardiac magnetic resonance (CMR) is another non-invasive imaging technique, which is used for the assessment of the heart chambers and myocardial tissue. Compared to echocardiography, CMR is superior in assessing myocardial tissue and left ventricular (LV) function. CMR is also used to identify ischemic and non-ischemic causes of heart failure (C. Liu et al., 2021). Although echocardiography and cardiac magnetic resonance (CMR) is the most used imaging techniques for the diagnosis of heart failure, with the increase in computation power, computed tomography angiography (CTA) is becoming a valuable diagnostic tool for heart failure. CTA provides detailed images of cardiac anatomy, which might be useful for diagnosing heart failure due to complex coronary abnormalities (Aziz et al., 2019).

Natriuretic peptides such as brain natriuretic peptide (BNP) and N-terminal pro-BNP (NT-proBNP) can be used as biomarkers of heart failure. In patients with heart failure, a

significant increase in BNP is observed, and it is proportional to the severity of heart failure. In patients who are at high risk of developing heart failure, such as those with diabetes mellitus or hypertension, natriuretic peptides can be used to assess the risk of developing heart failure (Vergani et al., 2024). Troponin is another important biomarker of heart failure, and increased levels of troponin indicate myocardial injury and heart failure. In heart failure, increased troponin levels strongly correlate with the underlying pathology (GHERASIM, 2019).

Heart failure management

Pharmacological treatment

The pharmacological management of HF includes several classes of drugs (Table 2). Some of these treatment options are considered first-line therapy regardless of other co-morbidities such as chronic kidney disease (CKD) (Rist et al., 2024).

Table 2. Pharmacological treatment options and clinical benefits in HF management

Drug Class	**Clinical Benefits**	**Patient Groups**
Beta-blockers	First-line therapy	All HF patients
Angiotensin-Converting Enzyme Inhibitors / Angiotensin II Receptor Blockers (ACEIs/ARBs)	First-line therapy	All HF patients
Mineralocorticoid Receptor Antagonists (MRAs)	First-line therapy	All HF patients
Angiotensin Receptor-Neprilysin Inhibitors (ARNIs)	Reduce HF hospitalizations	CKD
Sodium-Glucose Co-Transporter 2 Inhibitors (SGLT2 inhibitors)	Reduce cardiovascular death and HF hospitalizations	Elderly, CKD, diabetes, HFrEF
Soluble Guanylate Cyclase Stimulators (sGC stimulators)	Improve HF outcomes	CKD

The pharmacological management of heart failure depends on the severity, and often a combination of different classes of drugs is used (Table 2) (Safi et al., 2017). Beta-blockers are considered a first-line therapy for the management of heart failure due to their ability to reverse the hyperactivation of the renin angiotensin-aldosterone system and sympathetic nervous system (SNS) (Masarone et al., 2021). Among the three types of beta-receptors ($beta_1$, $beta_2$, and $beta_3$), $beta_1$ is mainly expressed in the heart, and activation of the $beta_1$ receptor leads to increased heart rate (positive chronotropic effect) and contractility (positive inotropic effect) (Safi et al., 2017). The prolonged activation of the sympathetic nervous system (SNS) after a cardiac insult results in increased plasma levels of epinephrine and norepinephrine (Masarone et al., 2021). The persistent activation of the $beta_1$ receptor by epinephrine and norepinephrine leads to cardiac beta-receptor dysfunction in heart failure. By blocking the $beta_1$ receptor, beta-blockers inhibit the chronotropic and inotropic effects (Farzam & Jan, 2026). It is recommended to initiate treatment with beta-blockers at a low dose, and if needed, increase the dose slowly. The clinical benefits of beta-blockers in chronic heart failure are dose-dependent, and a higher dose is tolerable and provides better benefits (Niriayo et al., 2020). Only the selective $beta_1$ blockers (metoprolol and bisoprolol) and third-generation non-selective combined alpha and beta blockers (carvedilol) are recommended for the management of heart failure (Safi et al., 2017). The recommended daily target dose of metoprolol, bisoprolol, and carvedilol is 200 mg, 10 mg, and 50 mg, respectively (Niriayo et al., 2020).

The neuropeptide angiotensin II (Ang-II) plays an essential role in the development of essential hypertension; however, inhibition of Ang-II has additional benefits other than only lowering blood pressure (Shrimpton et al., 2020). Angiotensin-converting enzyme inhibitors (ACEIs), such as enalapril and lisinopril, and angiotensin II receptor blockers (ARBs), such as valsartan and losartan, are also considered first-line therapy in heart failure management. ACEIs decrease systolic wall stress, preload, and afterload, which results in improved cardiac output without an increase in heart rate (Herman et al., 2026). Angiotensin II causes vasoconstriction, reduces water and sodium excretion, stimulates cardiac myocyte hypertrophy, and inhibits norepinephrine reuptake. Angiotensin-

converting enzyme inhibitors (ACEIs) modulate the renin-angiotensin-aldosterone system and block the conversion of angiotensin I to angiotensin II. Decreased angiotensin II levels lead to an increase in sodium and water excretion and lower blood pressure (M. G. Khan, 2015). The principal binding site for angiotensin II is the G protein-coupled receptor Ang-II type 1 (AT1). Angiotensin II receptor blockers (ARBs) inhibit the binding of angiotensin II to the AT1 receptor. The physiological effects of ACEIs and ARBs also include a decrease in cardiac remodeling and fibrosis (Shrimpton et al., 2020). The benefits of angiotensin-converting enzyme inhibitors (ACEIs) and angiotensin II receptor blockers (ARBs) are dose dependent, with higher doses significantly reducing all-cause mortality in heart failure (M. S. Khan et al., 2017). Neprilysin inhibitors in combination with angiotensin II receptor blockers, also known as angiotensin receptor neprilysin inhibitors (ARNIs), reduce hospitalization due to heart failure (Shrimpton et al., 2020). The recommended daily dose of commonly used angiotensin-converting enzyme inhibitors (ACEIs) in heart failure, such as enalapril and lisinopril, is 10-15 mg once or twice daily and 2.5-5 mg once daily, respectively, and for widely used angiotensin II receptor blockers (ARBs), such as valsartan and losartan, it is 80-160 mg once daily and 25-50 mg once or twice daily, respectively (M. S. Khan et al., 2017).

Mineralocorticoid receptor antagonists (MRAs), such as spironolactone and eplerenone, play a vital role in the management of heart failure, particularly in heart failure with reduced ejection fraction (HFrEF) (Y. Zhang et al., 2025). The overactivation of the renin-angiotensin-aldosterone system (RAAS) due to renal hypoperfusion caused by decreased cardiac output increases aldosterone secretion (Sica, 2015). Increased aldosterone secretion worsens the progression of heart failure by acting on the mineralocorticoid receptor, as overexpression of aldosterone causes electrolyte imbalance, water retention, myocardial fibrosis and remodeling, endothelial dysfunction, and arrhythmia (Zannad et al., 2012). The current guidelines for managing heart failure recommend the early administration of mineralocorticoid receptor antagonists (MRAs) in cases of heart failure with reduced ejection fraction (HFrEF). Additionally, it is advised to combine MRAs with sodium-glucose cotransporter 2 inhibitors (SGLT2i) in female patients, irrespective of their left ventricular

ejection fraction (LVEF). For male patients on SGLT2i, the addition of MRAs is suggested if the LVEF is below 55–60% (Sethi et al., 2026). Hyperkalemia is most common and often fatal side effect with mineralocorticoid receptor antagonists (MRAs), particularly in patients with chronic kidney disease (CKD). Regular serum K^+ levels monitoring is recommended while using MRAs (Sica, 2015).

Sodium-glucose cotransporter 2 inhibitors (SGLT2i), such as empagliflozin, were developed for the management of type 2 diabetes; however, this class of drugs is currently recommended for the management of heart failure regardless of diabetes (Talha et al., 2023). A significant reduction in cardiovascular adverse events, including hospitalization due to heart failure, was observed with SGLT2i (Epperson et al., 2024). Although the exact cardiovascular protective mechanism of sodium-glucose cotransporter-2 inhibitors (SGLT2i) is still under investigation, there are diverse proposed mechanisms, including increasing diuresis, improving cardiac energy metabolism, reducing inflammation, and promoting weight loss. SGLT2i also improve left ventricular ejection fraction (LVEF) and reduce myocardial remodeling (Lopez-Usina et al., 2024).

The low-density lipoprotein cholesterol (LDL-C) should be monitored regularly after a myocardial infarction, and the target level of LDL-C should be less then 70 mg/dl. Through numerous randomized controlled trials and epidemiological studies, the relationship between high levels of low-density lipoprotein cholesterol (LDL-C) and cardiovascular disease has been established (Grundy et al., 2019). The use of statins at a higher intensity is associated with better LDL-C management than moderate-intensity statins (Cholesterol Treatment Trialists' (Ctt) Collaboration, 2010). It is recommended to start high-intensity statin therapy after a myocardial infarction, and if the expected low-density lipoprotein cholesterol (LDL-C) level is not achieved with statin monotherapy, other therapies that also reduce LDL-C, such as ezetimibe, could be added to statins (Grundy et al., 2019). There are some statin-intolerant patients who cannot use statin medication due to some side effect, bempedoic acid is recommended for lipid management. Bempedoic acid is an effective therapy for lowering low-density lipoprotein cholesterol (LDL-C) and risk of cardiovascular diseases (Nissen et al., 2023).

Lifestyle modification

Low sodium diets are one of the most recommended non-pharmacological interventions used together with the pharmacological treatment options for heart failure. In theory, excessive sodium intake can cause fluid overload, which may worsen the progression of heart failure (Patel & Joseph, 2020). However, the study of dietary intervention under 100 mmol in heart failure (SODIUM-HF), which was an international open-label randomized control trial, did not find any significant reduction in cardiovascular-related hospitalization in heart failure patients following a low sodium diet (less then 1500 mg/day) (Ezekowitz et al., 2022). Moreover, low sodium diets have no positive effects on the quality of life (QoL) and mortality of heart failure patients (C. Zhu et al., 2022). There is much variability in the outcomes from the studies on dietary sodium intake and its impact on heart failure because most studies rely on self-reports from the patients, which might not be accurate due to poor dietary sodium adherence among heart failure patients (Basuray et al., 2015). However, the Dietary Approaches to Stop Hypertension (DASH) diet, which is low in sodium, red and processed meat, and sugar and includes whole grains, fruits, vegetables, low-fat dairy, nuts, and legumes, is associated with a lower risk of heart failure (Ibsen et al., 2022).

Smoking is one of the major risk factors associated with cardiovascular diseases, and after an acute myocardial infarction (AMI), smoking cessation is associated with significant reduction in mortality. After an AMI, even without complete cessation of smoking, the beneficial effects of reducing the number of cigarettes smoked daily can be observed in the reduced mortality rate by 18% (Gerber et al., 2009). It could be difficult for patients who are addicted to tobacco to stop smoking completely or even reduce the number of cigarettes they smoke daily. Behavioral support and nicotine replacement therapies have been found to be beneficial for smoking cessation (Stead et al., 2016). The majority of hospitalized patients after an acute coronary syndrome (ACS) do not stop smoking, and other comorbid conditions such as depression and chronic lung disease can further increase the odds of smoking cessation (Lovatt et al., 2021). Studies have shown that pharmacotherapy with

varenicline and bupropion combined with patient counseling is an effective strategy for smoking cessation in patients with cardiovascular disease (Suissa et al., 2017).

Zebrafish

The zebrafish (*Danio rerio*) is a well-established model organism in biomedical research. Comparative genomic studies estimated that 70% of human genes have at least one zebrafish orthologue, and 84% of disease-causing genes in humans have a zebrafish counterpart. However, this high number of similarities does not always translate to complete functional conservation, as some genes may perform different roles in zebrafish compared to humans, which can affect the applicability of zebrafish models in studying human diseases (Siddiqui et al., 2025).

Zebrafish are a popular animal model because they have some advantages, such as a fully sequenced genome, ease of genetic manipulation, external fertilization, rapid embryonic development, high fecundity, and short generation time (Teame et al., 2019).

Zebrafish as a model for cardiovascular diseases

The zebrafish (*Danio rerio*) has become a versatile model for cardiovascular research and drug development due to the genetic conservation and capacity to perform large-scale drug and genetic screening. Although zebrafish have a simplified cardiovascular system, it shares similarities with the mammalian cardiovascular system, and with their transparent embryos, different microscopic techniques can be applied to visualize the development of heart diseases (Angom & Nakka, 2024).

The heart development in zebrafish starts in the blastula phase and resembles the heart formation in early mammals. The zebrafish heart at 48 hours post fertilization is morphologically and physiologically comparable to a human embryo that is 35 days old. The zebrafish embryos can survive without connective circulation, as they can intake required oxygen through diffusion, which allows the heart to develop for extensive phenotypic assessment (Lu et al., 2020).

The first functioning organ during zebrafish embryonic development is the heart. The zebrafish heart can be divided into four separate components: the sinus venosus, one atrium, one ventricle, and the bulbus arteriosus (Singleman & Holtzman, 2012). The atrium and ventricle are the only parts of the heart that are considered chambers in zebrafish. This is because they can contract and have valves at both the entrance and exit (Hoareau et al., 2022). Although the zebrafish heart lacks complex pulmonary vasculature, the early development of the heart and the pumping function is similar between zebrafish and humans (Angom et al., 2025). In zebrafish simplified circulation the deoxygenated blood enters the atrium from the sinus venosus. The deoxygenated blood is collected from the veins and enters the sinus venosus before it enters the atrium. The deoxygenated blood then enters the ventricle, and the bulbus arteriosus guides the blood to the ventral aorta from the ventricle. The deoxygenated blood then enters the afferent branchial arteries, which lead the blood to the gills to be oxygenated. The efferent branchial arteries receive the oxygenated blood from the gills, which is then collected in the dorsal aorta, and oxygenated blood is distributed to the rest of the body (Hoareau et al., 2022).

There are high similarities in the electrocardiography (ECG) of zebrafish and human hearts. Zebrafish embryos from 3 days post fertilization (dpf) exhibit a similar ECG profile (Bowley et al., 2022). The basal heart rate of adult zebrafish at 28°C is 120-130 beats/minute, which is considered comparable to humans. In the ECG profile of zebrafish, similar to humans, there is a distinct P-wave. The QRS complex and T wave are observed (Verkerk & Remme, 2012). The cardiac action potential in both zebrafish and humans has a long plateau phase, and the major current systems, both inward and outward, are qualitatively similar in zebrafish and human hearts (Vornanen & Hassinen, 2016). The QT interval in zebrafish is highly similar to humans, and as a result, zebrafish is widely used as a model organism for assessing drug-induced QT prolongation (Y. Zhao et al., 2019).

Heart failure can be defined and quantified in various ways in zebrafish. Optical translucency in the zebrafish embryos permits the use of a normal stereomicroscope to assess cardiac function, whereas an electrocardiogram is required for adult zebrafish.

Fractional shortening (FS%) is commonly used as a measurement to assess cardiac function (Narumanchi et al., 2021).

$$FS\% = \frac{Diastolic\ length - Systolic\ length}{Diastolic\ length} \times 100\%$$

The hypoxia-induced zebrafish larval cardiac model has several advantages for studying myocardial infarction. This model is a higher throughput alternative to the mouse model. The complexity of the whole organism is retained in the zebrafish larval model, which makes it a more realistic alternative than organoids and 2D cell culture. Increased pigmentation in the larval body wall can be a disadvantage, as it can reduce the ability to measure heart function. This limitation can be mitigated by using a pigment mutation strain such as Casper (Burggren et al., 2024).

The embryonic cardiac development in zebrafish is rapid, and heart function can be easily observed. This rapid development, coupled with the similarities between zebrafish and mammalian hearts, makes zebrafish a useful model organism for studying human heart disease (Narumanchi et al., 2021). Due to similarities in the heart rate and comparable QT prolongation, the cardiovascular physiology is translatable between zebrafish and humans (Burggren et al., 2024).

Zebrafish heart regeneration

The zebrafish heart possesses remarkable regeneration capacity after a heart injury, similar to some other nonmammalian species such as frogs and axolotls. The heart regeneration capacity varies in vertebrates. Although the heart regeneration capacity is mostly lost in adult mammals, the neonatal mouse heart has the ability to regenerate in the first seven days after birth. Hence, the study of zebrafish and mouse hearts is important to understand the underlying mechanism of heart regeneration after a cardiac injury (Begeman & Kang, 2018).

The cardiomyocytes are mostly diploid in zebrafish, whereas the adult mammalian cardiomyocytes are primarily polyploid, which limits the heart regeneration capacity in

adult mammals. Diploid cells have a pair of homologous chromosomes, while polyploid cells can arise when the diploid cells go through DNA replication without cytokinesis, resulting in more than two complete sets of chromosomes. As a result of polyploidization, the cells might be terminally differentiated and exit the cell cycle (González-Rosa et al., 2018). The presence of polyploid cardiomyocytes correlates with the regenerating capacity of the heart, as observed in different strains of mice containing a variable number of polyploid cardiomyocytes, with a higher number of polyploid cardiomyocytes leading to decreased proliferation of the cardiomyocytes after injury. A similar correlation is also observed in zebrafish (Travisano & Lien, 2025).

In adult mammals, most cardiomyocytes are polyploid, and in species that have a high heart regeneration capacity, such as zebrafish, the cardiomyocytes are mostly diploid. In neonatal rodents, the cardiomyocytes transition from diploid to polyploid within the first seven days of their life, resulting in more than 90 percent polyploid cardiomyocytes. In humans, 90 percent of the cardiomyocytes also transition from diploid to polyploid within the first 20 years of life (González-Rosa et al., 2018). The adult mammalian cardiomyocyte and endothelial cells lose their ability to reactivate genes involved in proliferation, which leads to loss of regeneration after a cardiac injury (Begeman & Kang, 2018). The loss of the regeneration capacity of the heart coincides with the polyploidization of the cardiomyocytes, and studies have found that more than 50 percent of the cardiomyocytes need to be diploid for successful heart regeneration. In zebrafish, the inhibition of cytokinesis in the cardiomyocytes leads to polyploidization and loss of heart regeneration capacity (Travisano & Lien, 2025). The cardiomyocytes surrounding the wound after a cardiac injury divide 1-2 times to regenerate myocardium; therefore, if the number of diploid cells decreases and polyploid cells, which are proliferation-compromised, increase, the zebrafish heart regeneration capacity also decreases (González-Rosa et al., 2018).

The hearts of zebrafish, mice, and humans are composed of various cell types. The cardiomyocytes account for 33-49%, 25-35%, and 30-40% in human, mouse, and zebrafish hearts, respectively. The other cell types in the heart are fibroblasts, endothelial cells,

smooth muscle cells, and immune cells. These diverse cell types also play a crucial role in the regeneration process of the heart (Travisano & Lien, 2025).

The epicardial cells are activated after a cardiac injury and play an important role in zebrafish heart regeneration. The activated epicardial cells deposit collagens and fibronectin in the injured area for heart regeneration, re-enter the cell cycle, and re-express developmental genes. In mammals, the mobilization of epicardial cells improve heart regeneration. The activated epithelial progenitor cells (aEPC) from the epicardium migrate to the site of cardiac injury for wound healing (Weinberger et al., 2024). The activated epithelial progenitor cells (aEPC) undergo epithelial-mesenchymal transition (EMT) during heart regeneration in zebrafish, and disruption of this process leads to impaired heart regeneration. In adult mammals, the epicardial cells exhibit negligible R(EMT) after a cardiac injury and during embryonic development phase; disruption in EMT results in congenital heart defects in mice. The activated epithelial progenitor cells (aEPCs) are a potential target for the study of heart regeneration in adult mammals (Xia et al., 2022).

After a cardiac injury, fibroblasts deposit extracellular matrix (ECM), leading to cardiac fibrosis, which is an essential step for cardiac tissue repair. In mammals the ECM is not degraded when it has been deposited after myocardial infarction, whereas in zebrafish this fibrosis is transient, and studies have shown that the reduction in fibroblast ECM production is necessary for fibrosis regression. In the early stage of heart regeneration after a heart injury, fibrosis is essential, and a decrease in extracellular matrix (ECM)-producing cells leads to impaired cardiomyocyte proliferation (Sánchez-Iranzo et al., 2018). The fibroblasts in zebrafish have the ability to switch between reparative and fibrotic states, which is essential for reducing fibrosis and improving heart regeneration (Hu et al., 2022).

CRISPR as a gene-editing tool in zebrafish

Clustered regularly interspaced short palindromic repeats (CRISPR) technology is now being used widely, but it also faces various controversies due to the use of different animal models and cell lines (Moreno-Sánchez et al., 2025). Zebrafish has become an important model for CRISPR technologies due to various advantages, such as transparent embryos

and the short time requirement for their reproductive cycle. Although the model has been used since the 1980s, it was very time-consuming and laborious work to induce mutagenesis before CRISPR/Cas9 was introduced to use in this model, and now it is an efficient model for gene knockout studies (Wijerathna et al., 2024).

Sequencing technologies have advanced significantly, resulting in a large amount of genomic data; however, we still lack sufficient functional genomics data to characterize the genes, and it is estimated that around 30% of human gene functions remain unknown. The existence of noncoding genes causes further disadvantages in this regard. CRISPR/Cas9 provides a simplified way of addressing this issue (Varshney & Burgess, 2025). The efficiency and versatility of CRISPR/Cas9 made it an effective gene editing tool in zebrafish, and currently it is being extensively used for functional genomics studies, modeling cardiovascular diseases, and investigating the regeneration capacity of the zebrafish heart (Apolínová et al., 2024).

Targeted genetic mutation with efficiency similar to using zinc finger nucleases (ZFNs) and transcription activator-like effector nucleases (TALENs) can be achieved with the CRISPR/Cas9 system in zebrafish embryos (Hwang et al., 2013). Bi-allele mutation can be induced with the CRISPR/Cas9 system in the zebrafish F0 generation, which allows for rapid phenotype analysis with a 75-99% mutagenesis rate (Jao et al., 2013). It is possible to target multiple genes with the CRISPR/Cas9 system in zebrafish, which can be used to model multifactorial diseases and study the polygenic nature of disease (Angom et al., 2025). Furthermore, prime editing and base editing with CRISPR/Cas9 allow more precise gene editing (Kantor et al., 2020).

Gene targets

The target genes were selected based on a previous study (Huttunen et al., 2024) conducted at the Zebrafish Core at Turku Bioscience Centre. In the study, zebrafish embryos were treated with Empagliflozin prior to hypoxia exposure. Empagliflozin is a sodium glucose co-transporter 2 (SGLT2) inhibitor. In response to the Empagliflozin treatment, decreased expression of matrix metalloproteinase 13a *(mmp13a)* was

observed. Improvement in fractional shortening (FS%) was also observed in both the empagliflozin-treated and MMP13 inhibitor-treated groups.

The expression of sodium glucose co-transporter 1 (SGLT1) is higher (approximately 10-fold) in human heart compared to the kidneys (Zhou et al., 2003). However, SGLT2 expression in the heart is relatively low. Therefore, the cardioprotective effects of SGLT2 inhibitors might be mediated through pleiotropic mechanisms (Huttunen et al., 2024). The cardioprotective effect of empagliflozin was also observed in SGLT2 knockout mice, suggesting the beneficial effect on the heart is not SGLT2 dependent (Chen et al., 2023).

In this study, we aimed to further investigate the effect of *slc5a1* (Solute Carrier Family 5 Member 1*)*, *slc5a2* (Solute Carrier Family 5 Member 2), *mmp13a* (Matrix Metalloproteinase 13a), and *mmp13b* (Matrix Metalloproteinase 13b) gene knockout using CRISPR/Cas9 on heart failure in zebrafish embryos.

slc5a1

The *slc5a1* gene (ZDB-GENE-040426-1524) in zebrafish encodes a protein-coding gene and is located on chromosome 10 (GRCz12tu assembly). The protein in zebrafish is predicted to function as a D-glucose:sodium symporter, which plays a role in sodium ion and monoatomic ion transport. This gene is expressed in the digestive system and pronephric duct, and the encoded protein is localized at the apical plasma membrane of zebrafish. The zebrafish *slc5a1* gene is orthologous to the human *SLC5A1* gene, and in humans, *SLC5A1 is* involved in glucose-galactose malabsorption (Bradford et al., 2022).

The expression of *the slc5a1* (Figure 2) gene in zebrafish was detected in the endoderm, gut, PGCs, and pronephros clusters. The expression becomes more prominent at later developmental stages (84-120 hpf). The highest mean expression levels (log2 > 1.00) were observed in the endoderm and gut clusters. Minimal to no expression was detected in cardiac-related clusters such as the heart. The low expression seen in the heart-related clusters is consistent with the low heart expression reported in previous studies (Sur et al., 2023).

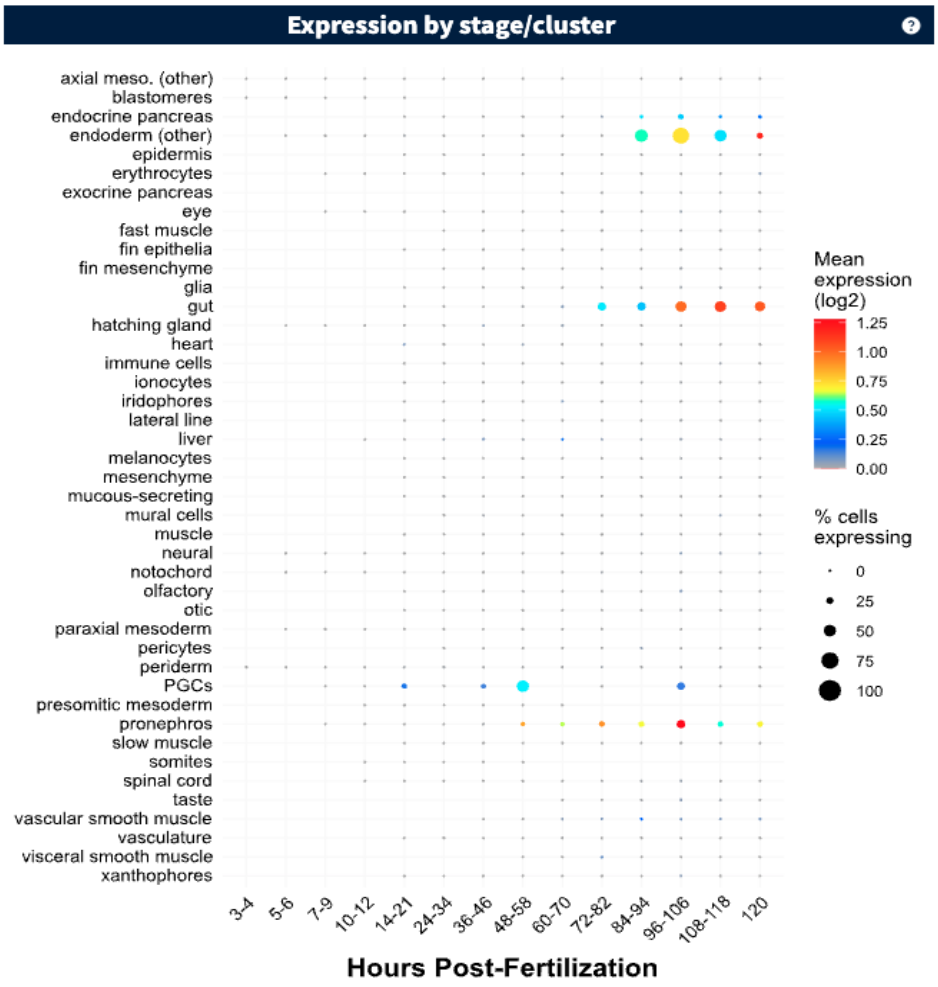

Figure 2. *Expression pattern of slc5a1 across developmental stages and cell clusters in zebrafish embryos. The gene expression was detected primarily in the endoderm, gut, PGCs, and pronephros clusters. Data obtained from Daniocell (https://daniocell.nichd.nih.gov/gene/S/slc5a1/slc5a1.html) (Sur et al., 2023).*

slc5a2

The *slc5a2* gene (ZDB-GENE-040426-2498) in zebrafish encodes a protein-coding gene located on chromosome 15 (GRCz12tu assembly). Similar to the zebrafish *slc5a1*, the encoded protein is predicted to function as a D-glucose:sodium symporter and is involved in sodium ion transport, localized at the apical plasma membrane. In zebrafish the gene is expressed in the polster, pronephric proximal convoluted tubule, and hatching gland. The zebrafish *slc5a2* gene is orthologous to the human *SLC5A2* gene. *SLC5A2* is involved in renal glycosuria and familial renal glucosuria in humans (Bradford et al., 2022).

The expression of *slc5a2* (Figure 3) in zebrafish was detected exclusively in the pronephros cluster, with no notable expression observed in any other cell cluster. Expression began at 48-58 hpf with low levels and progressively increased and reached its highest mean expression levels (log2 > 1.5-2.0) between 96 and 120 hpf. No expression was observed in the heart cluster throughout all developmental stages (Sur et al., 2023).

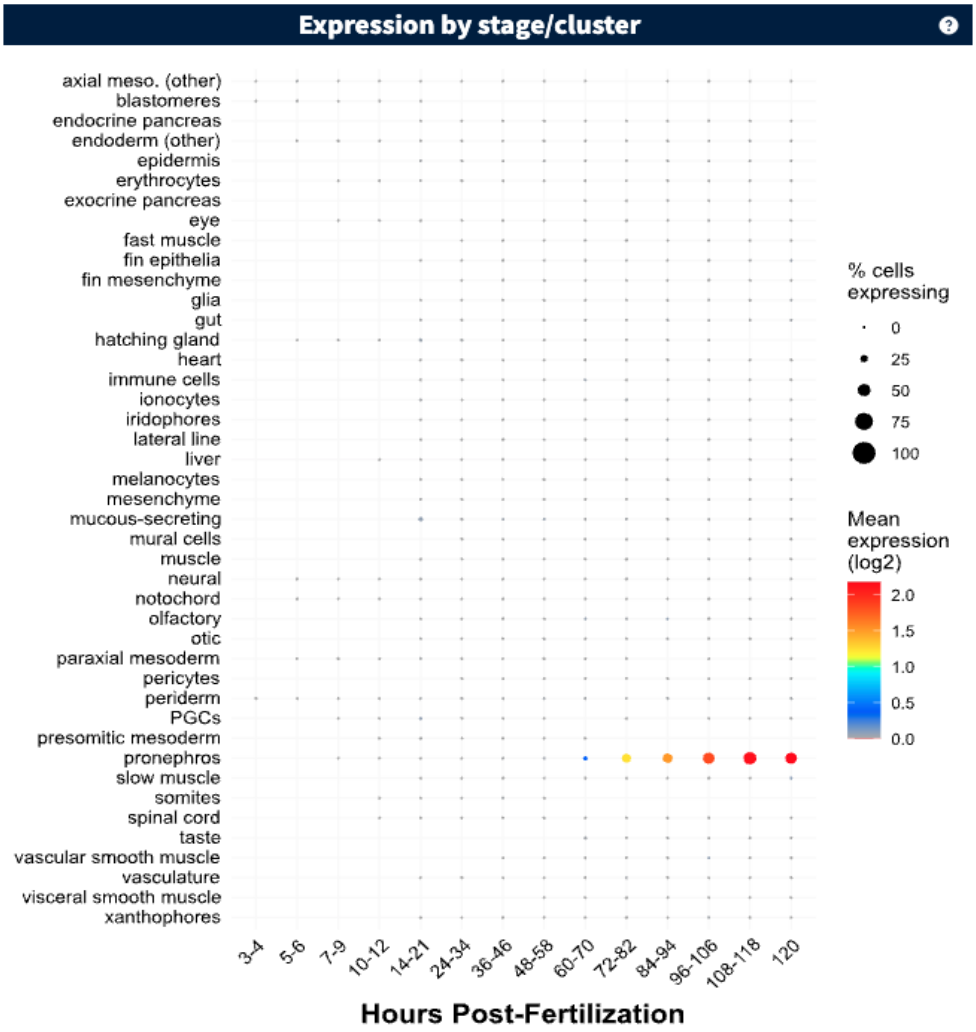

Figure 3. *Expression pattern of slc5a2 across developmental stages and cell clusters in zebrafish embryos, showing exclusive expression in the pronephros cluster. Data obtained from Daniocell (https://daniocell.nichd.nih.gov/gene/S/slc5a2/slc5a2.html) (Sur et al., 2023).*

mmp13a

The *mmp13a* gene (ZDB-GENE-031202-2), also known as matrix metallopeptidase 13a, is a protein-coding gene located on chromosome 10 in zebrafish. The gene is expressed in zebrafish in the heart, leukocytes, post-vent region, and intermediate cell mass of mesoderm, and the encoded protein acts upstream of or within macrophage chemotaxis. The zebrafish *mmp13a* is orthologous to the human *MMP13* gene. In humans, *MMP13 is*

involved in various disease conditions, including artery disease, anodontia, and bone disease (Bradford et al., 2022).

The expression *mmp13a* gene in zebrafish was detected in immune cells in the overall cell cluster analysis (Figure 4), with the highest mean expression (log2 > 3.0) observed at 14-21 hpf, followed by sustained expression throughout 24-120 hpf. Prominent expression was observed in granulocytes in the hematopoietic subcluster from 36-46 hpf onwards, with high mean expression (log2 > 3.0-5.0) sustained until 120 hpf. Expression was also detected in macrophages, hematopoietic stem cells, fin epidermis, and visceral smooth muscle, heart myocardium, and heart epicardium subclusters (Sur et al., 2023).

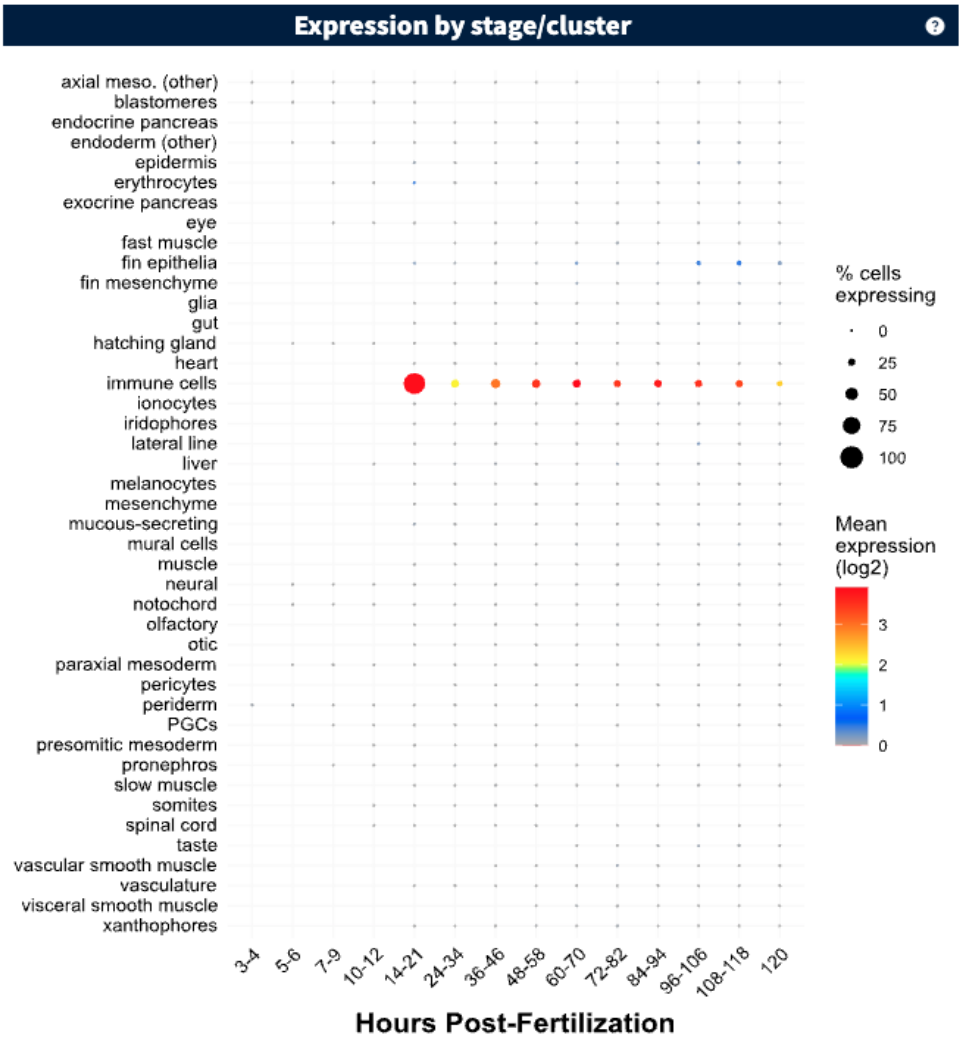

Figure 4. *Expression pattern of mmp13a across developmental stages and cell clusters in zebrafish embryos. mmp13a expression was predominantly detected in immune cells. Data obtained from Daniocell (https://daniocell.nichd.nih.gov/gene/M/mmp13a/mmp13a.html) (Sur et al., 2023).*

mmp13b

The mmp13b (ZDB-GENE-030131-6152) gene, also known as matrix metallopeptidase 13b in zebrafish, is a protein-coding gene located on chromosome 15 (GRCz12tu assembly). The encoded protein in zebrafish is predicted to function as a metalloendopeptidase. This gene is involved in the collagen catabolic process and extracellular matrix organization and is localized in the extracellular region and extracellular space. The *mmp13b* gene in

zebrafish is expressed in both the caudal fin and the posterior cardinal vein. The zebrafish *mmp13b* is orthologous to the human *MMP13* gene (Bradford et al., 2022). An overall low expression profile was observed in the expression pattern of the *mmp13b* gene across zebrafish developmental stages (Figure 5). Expression was detected (log2 < 0.08) primarily in fin epithelia at 14-21 hpf in the overall cell cluster analysis. No detectable expression was observed in cardiac-related clusters (Sur et al., 2023).

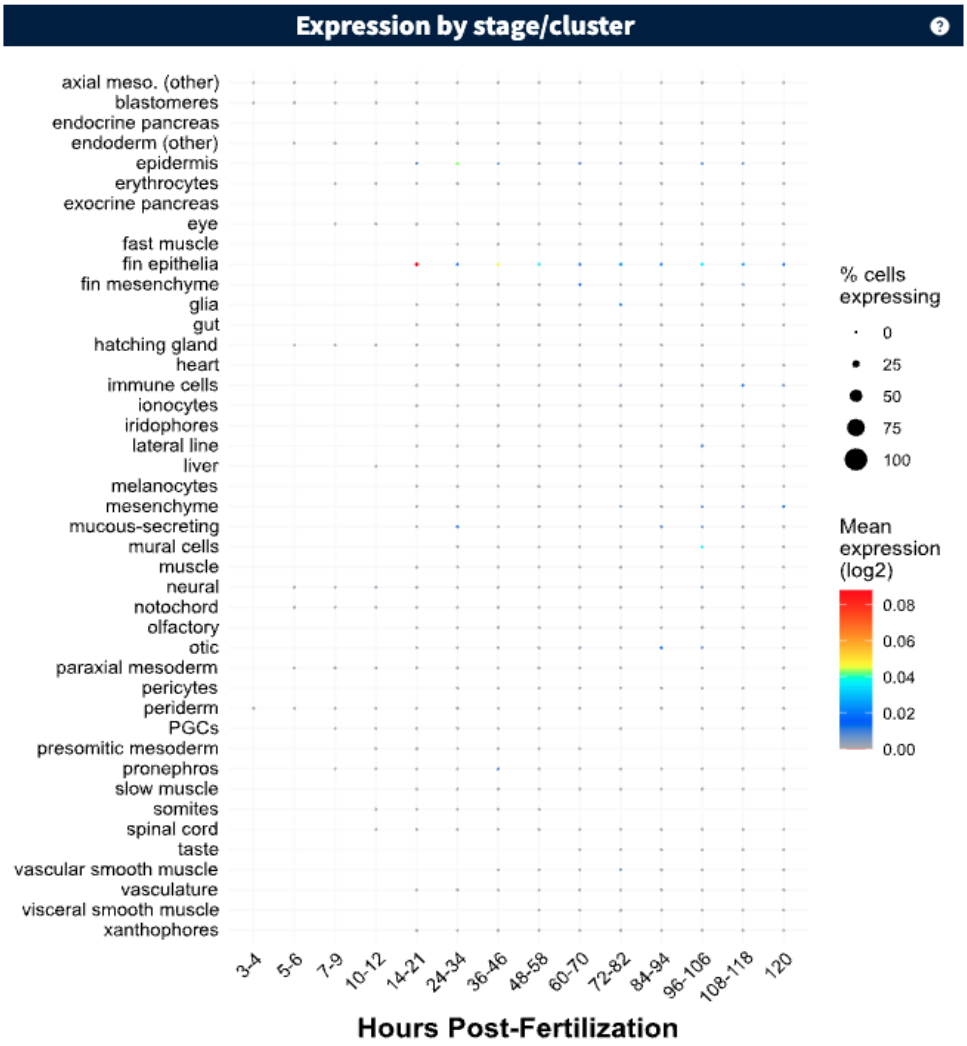

Figure 5. *Expression pattern of mmp13b across developmental stages and cell clusters in zebrafish embryos. mmp13b expression was predominantly detected in fin epithelia at early stages (14-21 hpf). Data obtained from Daniocell (https://daniocell.nichd.nih.gov/gene/M/mmp13b/mmp13b.html) (Sur et al., 2023).*

Molecular mechanism of hypoxic response

The cellular adaptive response in a hypoxic condition is mediated by a transcription factor known as hypoxia-inducible factor α (HIF-α). As this response is evolutionarily conserved, zebrafish can be used as a model organism to study the cellular responses to hypoxia (Greenald et al., 2015).

The level of HIF-α is controlled post-translationally. When sufficient oxygen is available, the HIF-α is hydroxylated by prolyl hydroxylase domain-containing proteins (PHDs) and factor-inhibiting HIF (FIH) (He et al., 2017). The hydroxylated products subsequently bind to the von Hippel-Lindau tumor suppressor (pVHL) protein for proteasomal degradation (Jopling et al., 2012). Oxygen is needed for the hydroxylase activity of PHD enzymes, and during hypoxia, this enzymatic activity is reduced, leading to HIF-α stabilization. Stable HIF-α forms a heterodimeric complex with HIF-β, and this complex transcribes hypoxia response element (HRE)-containing genes in the regulatory regions (S. & Santhakumar, 2025).

HIF-1α activates many important genes and affects many physiological processes. In the cellular adaptive response under hypoxia, HIF-1α activates vascular endothelial growth factor (VEGF), which promotes angiogenesis. To increase the supply of oxygen and nutrients, HIF-1α also promotes the expression of extracellular matrix (ECM) remodeling proteins (Wei et al., 2022).

The myocardium has a high energy demand and can use different energy sources for oxidative phosphorylation to produce the required ATP. Glucose is used when the blood glucose level is high, otherwise, the main substrate is free fatty acids (FFAs). During a hypoxic event, e.g., myocardial ischemia, the energy supply from oxidative metabolism is not sufficient, and a switch to an anaerobic glycolytic metabolic pathway occurs. This anaerobic pathway produces less ATP and is less energy efficient (García-Ropero et al., 2019).

The metabolic shift in hypoxic conditions from oxidative to glycolytic metabolism is mediated through the upregulation of glucose transporter-1 (GLUT1), glucose transporter-3

(GLUT3), and glycolysis-related enzymes by active HIF-1α (Taylor & Scholz, 2022). During this anaerobic metabolism, pyruvate is produced, which is further metabolized to lactate, and accumulation of lactate can lead to intracellular acidosis (Wei et al., 2022).

To counteract the increased cellular acidity after ischemia, the Na^+/H^+ exchanger 1 (NHE1) is activated, leading to proton extrusion. NHE1 is essential to regulate the pH homeostasis in cardiomyocytes (Lawrence et al., 2010). The activation of NHE1 causes intracellular Na^+ accumulation. During ischemia the Na^+/K^+ ATPase becomes inactive, and as a result the Na^+/Ca^{2+} exchanger is activated, leading to intracellular Ca^{2+} accumulation. This intracellular Ca^{2+} overload leads to myocardial injury and dysfunctions (Al-Shamasi et al., 2021).

Nitric oxide (NO) is produced by NO synthases (NOSs), which require oxygen for NO production, but under hypoxia, NO can be produced through the reduction of nitrite (NO_2^-) (Umbrello et al., 2013). NO plays an important role in cardiac development and controlling heart rate in zebrafish. In mammals, during hypoxia, NO modulates mitochondrial oxygen consumption and reduces ROS production. The NO/HIF-1α cardioprotective pathway is conserved throughout vertebrates. During ischemia, NOS genes are activated by HIF-1α in the mammalian myocardium, and a high concentration of NO stabilizes HIF-1α, promoting further NOS expression (Cerra et al., 2023). NO is also involved in NHE1 activation, with low physiological levels of NO activating NHE1 and high levels of NO inhibiting the exchanger (M. Zhang & Shah, 2020).

Zebrafish can tolerate and acclimate to hypoxic conditions through various complex physiological mechanisms. During the larval stage, zebrafish embryos can uptake oxygen through the skin by diffusion, and the larvae can even survive in a carbon monoxide (CO)-containing atmosphere (1-5%), where hemoglobin oxygen transport is totally blocked by CO (Kopp et al., 2014). Zebrafish exhibit variable oxygen sensitivity during different developmental stages, becoming more hypoxia intolerant as the developmental stage progresses (Cerra et al., 2023). In a study conducted by (Padilla & Roth, 2001), it was observed that during prolonged hypoxia or anoxia (0% O_2) exposure, zebrafish embryos can

enter a suspended animation stage during which cell division and motility are suspended. In the same study, 98.8% out of 85 embryos aged 13 hpf were alive after 24 hours of anoxia exposure, whereas only 4.4% out of 91 embryos aged 30 hpf and 0% out of 130 embryos aged 50 hpf were alive after 24 hours of anoxia exposure.

Conserved hypoxia response pathway between humans and zebrafish

In mammals, among the three isoforms of HIF-α (HIF-1α, HIF-2α, and HIF-3α), HIF-1α is primarily regulated under hypoxia. All vertebrates have at least three HIF-α subunits, and the HIF biology is well conserved across species. In zebrafish, the homologues of HIF-α are represented as Hif-1αa, Hif-1αb, Hif-2αa, Hif-2αb, Hif-3αa, and Hif-3αb, with Hif-1αb being the major hypoxic responsive homologue. Zebrafish Hif-1αb shares 57.8% amino acid identity with human HIF-1α (Elks et al., 2015). The most highly represented binding motif of HIF-1α in zebrafish is RCGTG, which is identical to that in human hypoxia response genes (Greenald et al., 2015).

There are three functional PHD enzymes in humans: PHD-1, PHD-2, and PHD-3. Zebrafish have one homologue for PHD-1 (Phd-1) and PHD-3 (Phd-3) and two homologues for PHD-2 (Phd-2a, Phd-2b), with Phd-3 being mostly upregulated in zebrafish under hypoxia (Elks et al., 2015). In *phd-3*-null zebrafish, the hypoxia-responsive genes were observed to be upregulated, and the mutant zebrafish were more resistant to hypoxia compared to wild-type zebrafish (Liao et al., 2023).

There is only one homologue of human VHL and FIH proteins in zebrafish, Vhl and Fih, sharing 52% and 79% amino acid similarity, respectively. There is 96% similarity in the enzymatically active domain between zebrafish Fih and human FIH protein (Elks et al., 2015). It was observed that the *fih*-null mutation makes zebrafish more hypoxia tolerant compared to wild-type zebrafish (Cai et al., 2018).

Aim of the study

The aim of this study was to evaluate the role of *slc5a1*, *slc5a2*, *mmp13a*, and *mmp13b* in a hypoxia-induced zebrafish embryo heart failure model using CRISPR/Cas9 gene knockout techniques. The role of sodium glucose cotransporter 2 (SGLT2) inhibitors in heart failure is being extensively studied, and other animal models, such as *the Slc5a2* knockout mice model, are also being used to understand the role of SGLT2 inhibitors such as empagliflozin in heart failure (Chen et al., 2024). Zebrafish embryo models are also widely used to understand the role of *slc5a2* in heart failure (Shi et al., 2017). The sodium glucose cotransporter 1 (SGLT1) is overexpressed in ischemic cardiomyopathy, and it has become an important drug target for heart failure treatment (Pérez-Carrillo et al., 2022). The role of MMP13 inhibitors in zebrafish heart regeneration has been evaluated with contradictory results, with higher doses of MMP13 inhibitors decreasing the zebrafish heart regeneration capacity (Xu et al., 2019). The target genes of this study are important drug targets for the treatment of heart failure, and they are currently being studied extensively. The goals of this study were to disrupt the genes in zebrafish embryos using CRISPR/Cas9 and analyze the heart physiology of the zebrafish embryos.

We hypothesized that CRISPR/Cas9-mediated knockout (KO) of candidate genes will improve cardiac function (FS%) in zebrafish embryos under hypoxia-induced heart failure conditions.

Summary

Heart failure is a complex clinical syndrome where the functional or structural impairment of the heart leads to the decreased ability of the heart to pump blood effectively to satisfy the metabolic need of the body (Warriner et al., 2015). Currently, around 64 million people are suffering from heart failure worldwide (Shahim et al., 2023). Although the prevalence of heart failure is 1-2% in adults, it can rise over 10% after the age of 70 (Ponikowski et al., 2016).

Myocardial infarction (MI) is considered the major cause for heart failure, and various non-invasive imaging techniques such as echocardiography and cardiac magnetic resonance (CMR) can be used for the clinical diagnosis of heart failure (Aziz et al., 2019).

The management of heart failure often includes a combination of drugs selected based on the severity of the condition and the presence of comorbidities such as diabetes and kidney disease (Rist et al., 2024). Changes in dietary habits is also a recommended non-pharmacological intervention in heart failure (Patel & Joseph, 2020).

Zebrafish is one of the most commonly used disease models for researching various diseases, including cardiovascular diseases such as heart failure (Burggren et al., 2024). The presence of disease-causing gene orthologs makes zebrafish a valuable disease model for assessing the role of different genes in various disease conditions (Siddiqui et al., 2025).

In this study we aimed to evaluate the role of *slc5a1*, *slc5a2*, *mmp13a*, and *mmp13b* in heart failure using a zebrafish embryo model with the CRISPR/Cas9-mediated gene knockout technique.

2. Results

The zebrafish embryos were injected with the CRISPR/Cas9 ribonucleoprotein (RNP) complex at the 1-4 cell stage to knock out the candidate genes, and with every candidate gene knockout, the *slc45a2 (*solute carrier family 45 member 2*)* gene was also knocked out. The *slc45a2* gene in zebrafish is expressed in the melanocytes, and disruption of the gene results in a hypopigmentation phenotype (Bradford et al., 2022). The hypopigmentation phenotype was used as a visual biomarker to select the embryos in which the microinjection was successful.

The embryos were imaged at 4 days post fertilization (4 dpf), and a 5-10 second heart movie was captured. The diameter of the zebrafish heart at diastole and systole was measured in ImageJ/Fiji, and the fractional shortening (FS%) of the heart was calculated with these two measurements.

There was no statistically significant difference between the groups in the first experiment at baseline, and the successful knockout of the candidate genes was confirmed with the TIDE (Tracking of Indels by Decomposition) analysis. In the second experiment, after 45 minutes of hypoxia exposure, the fractional shortening (FS%) in the *mmp13b* knockout group was significantly reduced compared to the negative control group, while in the *mmp13a* knockout group, a trend towards reduction, and in the *slc5a1* and *slc5a2* knockout groups, a trend towards improvement in the fractional shortening (FS%), was observed. Based on the results of 45 minutes of hypoxia exposure, it was decided to expose only the *slc5a1* and *slc5a2* knockout group to 60 minutes of hypoxia. A significant improvement in fractional shortening (FS%) was observed in both *slc5a1* and *slc5a2* knockout groups compared to the negative control group.

Baseline calculation

For baseline measurements, all groups (negative control (Neg. Ctrl), *slc5a1, slc5a2, mmp13a,* and *mmp13b*) were imaged at 4 dpf without hypoxia exposure at 3 dpf, and fractional shortening (FS%) was calculated. Individual FS% values for all groups are

provided in Supplementary Table 1. Only embryos exhibiting hypopigmentation were selected for imaging, while normally pigmented embryos were excluded.

Mean fractional shortening was similar across all groups (Neg. Ctrl (negative control): n (number of embryos) = 25, 15.99 ± 3.85%; *slc5a1*: n = 9, 15.49 ± 3.64%; *slc5a2*: n = 15, 17.78 ± 6.21%; *mmp13a*: n = 16, 13.89 ± 12.17%; *mmp13b*: n = 7, 14.46 ± 3.71%). Higher variability (SD = 12.17) was observed in the *mmp13a* knockout group compared to other groups (SD range: 3.64 - 6.21).

Normality of fractional shortening data was assessed for each group using the Shapiro-Wilk test. All groups were found to be normally distributed (Neg. Ctrl: W = 0.968, p = 0.598; *slc5a1*: W = 0.936, p = 0.540; *slc5a2*: W = 0.928, p = 0.257; *mmp13a*: W = 0.895, p = 0.067; *mmp13b*: W = 0.865, p = 0.166). Visual inspection of the histogram and Q-Q plot of model residuals (Supplementary Figure 1), as well as individual histograms and Q-Q plots for each group (Supplementary Figure 2), showed normality.

Homogeneity of variances was assessed using the Brown-Forsythe test (Levene's test based on median). The assumption of equal variances was violated ($F(4, 67) = 5.07$, $p = 0.001$); therefore, Welch's ANOVA was performed instead of the standard one-way ANOVA. No statistically significant difference in fractional shortening was found between groups ($F = 0.66$, $p = 0.611$, $\eta^2 = 0.04$) as shown in Figure 6; therefore, post-hoc analysis was not performed.

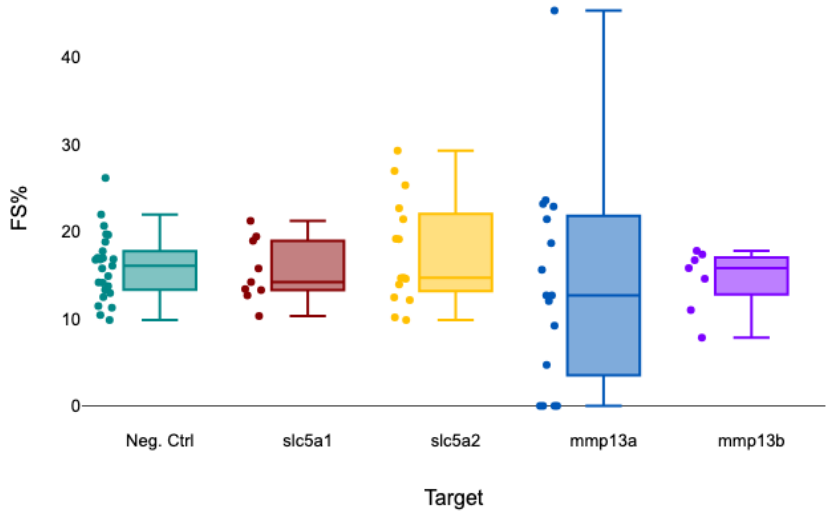

Figure 6. *Fractional shortening (FS%) of zebrafish embryos at 4 dpf in negative control and CRISPR/Cas9 knockout groups (slc5a1, slc5a2, mmp13a, and mmp13b). Data presented as boxplots with individual data points. No statistically significant difference was observed between groups (Welch's ANOVA, p = 0.611).*

TIDE analysis

In this study two CRISPR RNAs (crRNAs) were used to produce two guide RNAs (gRNAs) to knock out each candidate gene, and CRISPR knockout efficiency was verified using TIDE (Tracking of Indels by Decomposition) analysis for all target genes (Brinkman et al., 2014). Editing efficiencies were as follows: *mmp13a* (Supplementary Figure 3) demonstrated the highest efficiency at 86.3% (R^2 = 0.86), with a predominant -1 deletion (69.9%, $p < 0.001$) at the expected cut site (234 bp). *slc5a2* (Supplementary Figure 4) showed an efficiency of 59% (R^2 = 0.74), with predominant mutations of -1 deletion (19.6%) at the expected cut site (270 bp). *slc5a1* (Supplementary Figure 5) showed an efficiency of 42.2% (R^2 = 0.43) with multiple indels distributed across sizes at the expected cut site (205 bp). *mmp13b* (Supplementary Figure 6) demonstrated the lowest editing efficiency of 17.7% (R^2 = 0.21), with a predominant -8 deletion (8.7%) at the expected cut site (46 bp). The results of gene knockout efficacy are based on only one gRNA, and it is reasonable to assume that if we could consider both gRNAs, the actual efficacy would be higher.

45 minutes of hypoxia exposure

Zebrafish embryos in all groups (Neg. Ctrl, *slc5a1*, *slc5a2*, *mmp13a*, and *mmp13b*) were exposed to 45 minutes of hypoxia at 3 dpf, followed by imaging at 4 dpf to calculate fractional shortening (FS%). Raw FS% values for all groups are provided in Supplementary Table 2.

Mean fractional shortening following hypoxia exposure was similar across all groups (Neg. Ctrl: n = 18, 20.66 ± 5.60%; *slc5a1*: n = 22, 23.03 ± 3.46%; *slc5a2*: n = 15, 23.89 ± 3.67%; *mmp13a*: n = 8, 18.72 ± 5.05%; *mmp13b*: n = 10, 15.20 ± 4.37%). The *mmp13b* knockout group showed the lowest mean FS% compared to other groups. All groups were found to be normally distributed with the Shapiro-Wilk test (Neg. Ctrl: W = 0.958, p = 0.554; *slc5a1*: W = 0.963, p = 0.561; *slc5a2*: W = 0.967, p = 0.811; *mmp13a*: W = 0.937, p = 0.583; *mmp13b*: W = 0.959, p = 0.769). Normality was also observed with Q-Q plots and histograms (Supplementary Figure 7 & Supplementary Figure 8).

Homogeneity of variances was assessed using the Brown-Forsythe test (Levene's test based on median). The assumption of equal variances was met ($F(4, 68) = 1.24$, $p = 0.303$); therefore, a standard one-way ANOVA was performed. A statistically significant difference in fractional shortening was found between groups ($F(4, 68) = 7.65$, $p < 0.001$, $\eta^2 = 0.31$), as shown in Figure 7. Dunnett's post-hoc test revealed that only the *mmp13b* knockout group showed a statistically significant reduction in fractional shortening compared to the negative control (mean difference = -5.46%, p = 0.010). No significant differences were observed for *slc5a1* (p = 0.290), *slc5a2* (p = 0.132), or *mmp13a* (p = 0.711) knockout groups compared to the negative control.

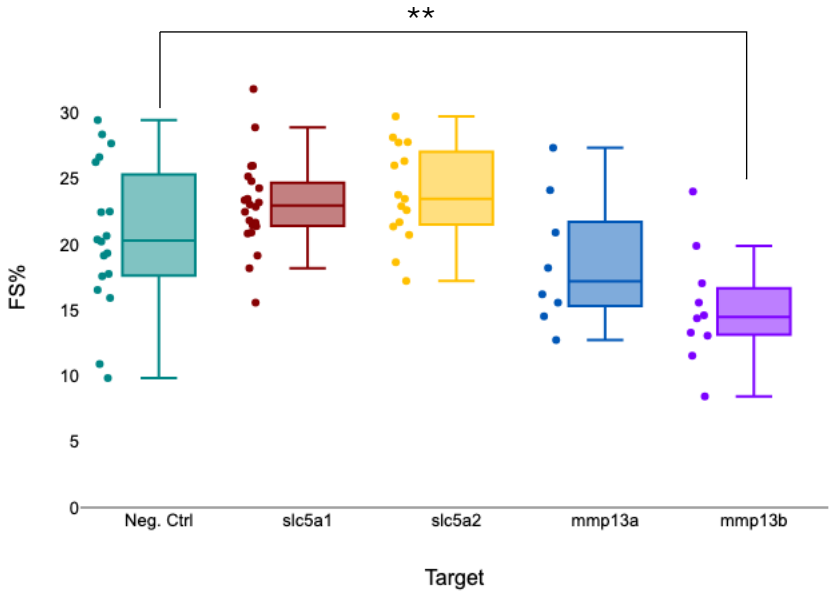

Figure 7. *Fractional shortening (FS%) of zebrafish embryos following 45 minutes of hypoxia exposure at 3 dpf. Data presented as boxplots with individual data points. Significant reduction in FS% is observed in the mmp13b knockout group (**p < 0.01) compared to the negative control (Dunnett's post hoc test).*

60 minutes of hypoxia exposure

Following 45 minutes of hypoxia exposure, a slight but non-statistically significant increase in fractional shortening (FS%) was observed in the *slc5a1* and *slc5a2* knockout groups. Therefore, hypoxia duration was extended to 60 minutes for these two groups to further investigate the effect on fractional shortening (FS%). For this experiment, approximately half of the negative control embryos were exposed to hypoxia while the remaining embryos were maintained under normoxic conditions throughout. Raw FS% values for all groups after 60 minutes of hypoxia exposure are provided in Supplementary Table 3.

Median fractional shortening following 60 minutes of hypoxia exposure was as follows (Neg. Ctrl_normoxia: n = 42, 17.76% (IQR = 4.62); Neg. Ctrl_hypoxia: n = 43, 15.33% (IQR = 4.66); *slc5a1*: n = 31, 18.89% (IQR = 5.85); *slc5a2*: n = 27, 18.80% (IQR = 3.94)). The negative control hypoxia group showed the lowest median FS% compared to other groups. Normality was assessed using the Shapiro-Wilk test. While Neg. Ctrl_normoxia, *slc5a1,* and *slc5a2* were found to be normally distributed (Neg. Ctrl_normoxia: n = 42, W = 0.967, p = 0.266; *slc5a1*: n = 31, W = 0.959, p = 0.282; *slc5a2*: n = 27, W = 0.960, p = 0.374), the

negative control hypoxia group violated the assumption of normality (Neg. Ctrl_hypoxia: n = 43, W = 0.904, p = 0.002). Normality was also assessed with Q-Q plots and histograms (Supplementary Figure 9 & Supplementary Figure 10).

As the assumption of normality was violated in the negative control hypoxia group, a Kruskal-Wallis test was performed instead of a standard one-way ANOVA. A statistically significant difference in fractional shortening was found between groups ($p < 0.001$), as shown in Figure 8. Dunn's post-hoc test with Bonferroni correction revealed statistically significant differences between the negative control hypoxia group and all other groups. Fractional shortening was significantly higher in the negative control normoxia group ($p = 0.009$), *slc5a1* knockout group ($p < 0.001$), and *slc5a2* knockout group ($p = 0.004$) compared to the negative control hypoxia group.

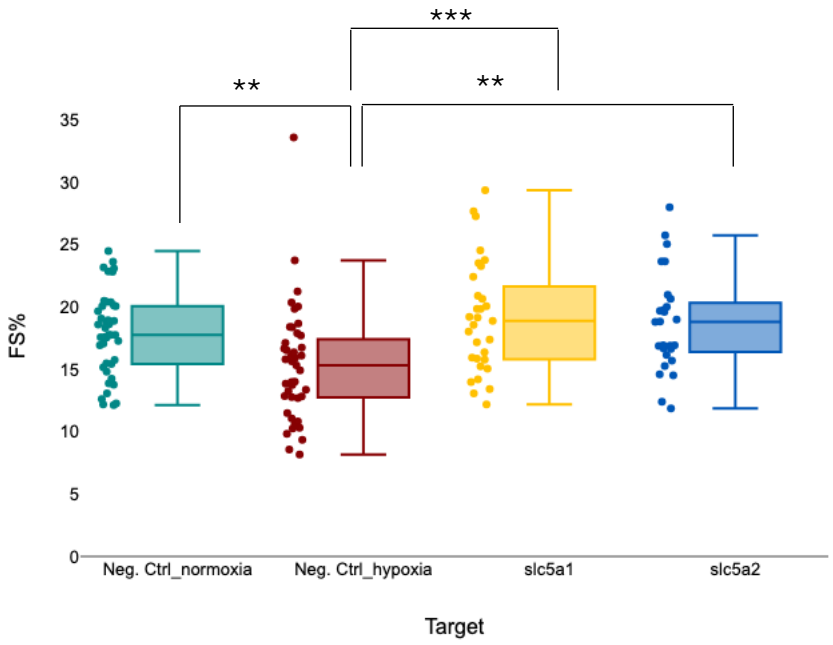

Figure 8. *Fractional shortening (FS%) of zebrafish embryos following 60 minutes of hypoxia exposure at 3 dpf. Data presented as boxplots with individual data points. Significant differences were observed between the negative control hypoxia group and all other groups (Kruskal-Wallis, $p < 0.001$; Dunn's post-hoc test: **$p < 0.01$, ***$p < 0.001$).*

3. Discussion

In this study, CRISPR/Cas9 gene editing technology was used to knockout *slc5a1*, *slc5a2*, *mmp13a,* and *mmp13b* genes in zebrafish embryos in the 1-4 cell stage. The embryos were exposed to hypoxia at 3 days post fertilization (dpf), and heart images were taken at 4 dpf to calculate the fractional shortening (FS%) of the heart. After 45 minutes of hypoxia exposure, a significant decrease in FS% was observed in the *mmp13b* group, and after 60 minutes of hypoxia exposure, significant improvement in FS% was observed in the *slc5a1* and *slc5a2* groups. A slight but not significant decrease in the FS% was observed in the *mmp13a* group after 45 minutes of hypoxia exposure.

The hypoxia-inducible factor α (HIF-α)-mediated cellular response to hypoxia is highly conserved in vertebrates, which makes zebrafish a suitable model organism to study the cellular adaptation after a hypoxic injury (Greenald et al., 2015). There are three isoforms of HIF-α in mammals, and the cellular response to hypoxia is primarily regulated by HIF-1α. Hif-1αb is the homologue of HIF-α in zebrafish that is primarily involved in the hypoxia response, and 57.8% shared amino acid identity is observed between human HIF-1α and zebrafish Hif-1αb (Elks et al., 2015). This well-conserved HIF biology between zebrafish and humans allows us to study and speculate about the human cardiomyocyte's response to hypoxia, which occurs during a myocardial infarction, by studying the zebrafish heart after a hypoxic injury.

CRISPR/Cas9-mediated gene knockout validation by TIDE

TIDE (Tracking of Indels by Decomposition) analysis is a computational method that uses Sanger sequencing data to evaluate the spectrum and frequency of CRISPR/Cas9-mediated small insertions and deletions (indels). TIDE is useful for analyzing gene editing efficacy in samples containing a mixture of wild-type DNA and DNA with a diverse range of indels; however, it may not fully capture the complexity of CRISPR editing efficacy, particularly in cases involving large deletions, inversions, or translocations. TIDE uses a non-negative linear modeling (NNLS) approach to determine which combination of indels,

when superimposed on the WT reference sequence, best explains the observed aberrant signal in the experimental trace (Brinkman et al., 2014). High-efficiency gene editing was observed in the *mmp13a* knockout group at 86.3% (R^2 = 0.86). Moderate efficacy was observed with *slc5a2* (59%, R^2 = 0.74) and *slc5a1* (42.2%, R^2 = 0.43) knockout groups. A low efficiency (17.7%, R^2 = 0.21) gene editing was observed with the *mmp13b* knockout group.

In this study we used two CRISPR RNAs (crRNAs) to produce two guide RNAs (gRNAs) to knockout each target gene. This two gRNAs for targeting the same gene approach during CRISPR/Cas9-mediated gene knockout increases confidence in producing loss-of-function alleles (Pauwels et al., 2018). It is reasonable to assume that the actual gene editing efficacy would be higher, as the TIDE application is only considering one gRNA-mediated gene knockout. In the case of *mmp13b*, the expected CRISPR cut site was at 46 bp, and the initial Sanger sequence reads might be of poor quality, which might explain the low gene editing efficacy.

slc5a1 and *slc5a2* knockout improved cardiac function in zebrafish embryos

In this study, improvement in fractional shortening (FS%) was observed in the *slc5a1* and *slc5a2* knockout zebrafish embryos after 60 minutes of hypoxia exposure at 3 days post fertilization. These results tie well with the previous study (Huttunen et al., 2024) conducted at the Zebrafish Core at the Turku Bioscience Centre, where empagliflozin, a sodium glucose cotransporter 2 (SGLT2) inhibitor, improved the FS% in the hypoxia-induced zebrafish heart failure model.

The slc5a1 and *slc5a2* genes in zebrafish is orthologous to human *SLC5A1* and *SLC5A2* genes, respectively. Both the *slc5a1* and *slc5a2* genes in zebrafish function as a D-glucose:sodium symporter. In zebrafish, *slc5a1* is expressed in the pronephros, gut, endoderm, and heart, whereas *slc5a2* is expressed predominantly in the pronephros (Bradford et al., 2022).

In humans, similar to zebrafish, the *SLC5A1* gene is widely distributed in the intestines, kidneys, and heart, and *SLC5A2* is expressed primarily in the renal proximal tubule. The sodium glucose transport ratio of SGLT1 is 2 Na^+:1 glucose and for SGLT2 the ratio is 1Na^+:1 glucose per cycle (Gyimesi et al., 2020). Approximately 97% of filtered glucose is reabsorbed by SGLT2, and only 3% is by SGLT1 in euglycemia. SGLT2 inhibitors can enhance the glucose reabsorption capacity of SGLT1 from ~3% to ~40-50% (Vallon, 2024). Individuals with loss-of-function mutations in the *SLC5A1* gene (SGLT1) exhibit glucose malabsorption from the intestine, and familial renal glucosuria, which is the excretion of 60–120 g of glucose in the urine daily, is observed in those with loss-of-function mutations in the *SLC5A2* gene (SGLT2) (Vallon & Verma, 2021). The involvement of SGLT2 and SGLT1 in glucose reabsorption explains the development of SGLT2 and SGLT1 inhibitors for glycemic control in diabetes, but the beneficial effects of SGLT2 and SGLT1 inhibitors in heart failure were observed later.

Myocardial infarction (MI) is considered the cause for developing heart failure, and heart failure conditions worsen after an acute myocardial infarction (AMI) (Jugdutt, 2012). Following hypoxic injury, the Na^+/H^+ exchanger 1 (NHE1) is activated to reduce the intracellular H^+ accumulation caused by the shift from oxidative to glycolytic metabolism, which leads to an increase in the intracellular Na^+ levels, and as the driving force for the sodium-calcium exchanger (NCX) is reversed, intracellular Ca^{2+} levels are increased. This Ca^{2+}overload induces inflammatory mediators such as TNFα and IL-6 and activates NADPH oxidase, leading to increased cytoplasmic ROS production (Y. Zhu et al., 2025). The regulation of intracellular pH by NHE1 activation may serve positively inotropic; however, prolonged activation of NHE1 leads to ischemia-reperfusion injury, cardiomyocyte death, and contractile dysfunction through Ca^{2+} overload (M. Zhang & Shah, 2020). NHE1 was found to be overexpressed in the myocardium of heart failure patients regardless of diabetes (Pérez-Carrillo et al., 2022). Inhibition of the sodium/hydrogen exchanger 1 (NHE1) was observed to decrease cytoplasmic Na^+ and Ca^{2+} concentrations, which increases mitochondrial Ca^{2+} levels and improves cardiomyocyte viability (Pérez-Carrillo et al., 2022). Nitric oxide (NO) also plays an important role in the activation of NHE1. At a low

physiological level of NO, NHE1 is activated, and high levels of NO deactivate it. NO modulates coronary flow, cardiomyocyte relaxation, and growth (M. Zhang & Shah, 2020). Inhibition of nitric oxide synthases (NOSs), which are the primary enzymes that produce NO, was found to completely counteract the cardioprotective effects of SGLT2 inhibitors such as empagliflozin (Chen et al., 2024).

The cardioprotective effects of SGLT2 inhibitors are thought to be mediated by inhibiting the Na^+/H^+ exchanger 1 (NHE1) in the cardiomyocytes as well as Na^+/H^+ exchanger 3 (NHE3) in the kidneys. The activation of NHE3 and SGLT2 is interdependent, as observed in NHE3 knockout mice, where SGLT2 expression and SGLT2 inhibitor-mediated urinary Na^+ excretion were reduced (Y. Zhu et al., 2025). This interdependent activation of SGLT2 and NHE3 might be one of the potential mechanisms that explains the beneficial effects of *slc5a2* knockout in the fractional shortening (FS%) of the zebrafish heart that we observed in this study.

The cardioprotective effects of the SGLT2 inhibitor empagliflozin in heart failure are independent of SGLT2, as observed in *Slc5a2* KO mice, where empagliflozin improved the cardiac function in heart failure. Inhibition of NHE1 also mimics the cardioprotective effects of empagliflozin, and no added benefits were observed with adding empagliflozin with NHE1 inhibition in heart failure (Chen et al., 2024), indicating an off-target effect of empagliflozin. In mice lacking SGLT2, higher renal expression of heme oxygenase-1 (HO-1), which is a tissue protective gene, is observed. In humans, inhibition of SGLT2 promotes erythropoietin (EPO) production, which helps improve heart failure outcomes through hematopoietic mechanisms (Vallon & Verma, 2021). In an aristolochic acid (AA)-induced zebrafish embryo heart failure model, Empagliflozin significantly reduced the functional cardiac changes associated with heart failure, and morpholino (MO)-mediated knockdown of *slc5a2* in zebrafish embryos exhibited similar cardioprotective changes mediated by empagliflozin in AA-induced heart failure (Shi et al., 2017). In this study we also observed an improvement in fractional shortening (FS%) in CRISPR/Cas9-mediated *slc5a2* knockout zebrafish embryos in a hypoxia induced heart failure model, further confirming the beneficial effects of SGLT2 inhibition in heart failure.

Under hypoxic conditions, the preferred substrate for ATP production is switched from fat to glucose, as the glycolytic ATP production is not dependent on oxygen (Ekanayake et al., 2020). SGLT2 inhibitors mimic a fasting condition by lowering blood glucose and can induce a shift from carbohydrate to lipid metabolism and the formation of ketone bodies in the liver (Vallon, 2024). Ketone bodies, β-hydroxybutyrate (BHOB) and acetoacetate, improve the energy efficiency of the heart, decrease ROS production, and slow HF progression (Ekanayake et al., 2020). Ketone oxidation is associated with improved heart failure outcomes in patients, and this mechanism of improved energy supply is also observed in failing murine hearts and porcine heart failure models. The starvation-like response of the SGLT2 inhibitors can induce autophagy, which improves systemic cellular defense and reduces oxidative stress (Vallon & Verma, 2021). SGLT2 inhibitors can also reduce fluid overload and hypertension, which improves heart failure outcomes (Vallon, 2024). This production of ketone bodies and improvement of cardiac energy supply might also be a potential mechanism for the improvement of fractional shortening (FS%) in the *slc5a2* and, to some extent, *slc5a1* knockout zebrafish embryos.

Overexpression of SGLT1 has been observed in patients with ischemic cardiomyopathy (Pérez-Carrillo et al., 2022). Overexpression of *Slc5a1* in mice was associated with chronic pressure overload leading to hypertrophic cardiac myopathy, cardiac remodeling, and interstitial fibrosis (Lin et al., 2021). Individuals with functionally damaged SGLT1 exhibit 23% and 30% relative risk reduction in type 2 diabetes mellitus (T2DM) and heart failure (HF), respectively, whereas functionally damaged SGLT2 is associated with less than 3% relative risk reduction for both T2DM and HF, and knockdown of SGLT1 in mice improves cell viability and protects against acute myocardial ischemia reperfusion injury and myocardial nitro-oxidative stress (Sayour et al., 2021). These findings indicate a role of SGLT1 in ischemic cardiomyopathy and make SGLT1 a potential drug target for heart failure management.

The direction and transport rate of SGLT1 is dependent on Na^+ concentration, and the direction is reversible. In the absence of glucose, SGLT1 can also function as a Na^+ uniporter (Gyimesi et al., 2020). In hypoxic conditions, intracellular Na^+ concentration is

increased by the activation of Na^+/H^+ exchanger 1 (NHE1), which leads to intracellular Ca^{2+} overload (Y. Zhu et al., 2025). Cardiomyocyte hypertrophy and oxidative stress mediated by intracellular Ca^{2+} overload can be reduced by SGLT1 inhibition and the shift of inflammatory M1 macrophages to anti-inflammatory M2 macrophages, and myocardial fibrosis suppression can also be significantly stimulated by the inhibition of SGLT1 (M. Zhao et al., 2023). The improvement in fractional shortening (FS%) that was observed in the *slc5a1* knockout group could be the results of decreased Na^+ levels in the cardiomyocytes of zebrafish embryos.

mmp13a and *mmp13b* knockout worsened cardiac function in zebrafish embryos

In the previous study (Huttunen et al., 2024), where zebrafish embryos were exposed to chemical hypoxia, the matrix metalloproteinase 13a (*mmp13a)* gene was downregulated in response to empagliflozin treatment, and treatment with an MMP13 inhibitor significantly improved the fractional shortening (FS%) in the zebrafish embryos exposed to chemical hypoxia. However, in this study, improvement in FS% was not observed in the *mmp13a* and *mmp13b* knockout zebrafish embryos when exposed to chemical hypoxia. After 45 minutes of hypoxia exposure, a significant decrease in the FS% was observed in the *mmp13b* knockout group, and a slight but not significant decrease was observed in the *mmp13a* knockout group compared to the negative control group. The difference between gene knockout and using an inhibitor might be the reason for these contradictory results.

The *mmp13a* and *mmp13b* genes in zebrafish is orthologous to the human *MMP13* gene, and they are paralogous to each other (Bradford et al., 2022). Teleosts, such as zebrafish, after their diversification as a lineage, underwent a third whole genome duplication (WGD) process (3R or TS-WGD) around 320–350 million years ago, which gave rise to the *mmp13a* and *mmp13b* paralogues in zebrafish. Initially the duplicated genes can perform the same function however, this also allows one copy of the gene to accumulate mutations, allowing regulatory divergence to occur (Angelakopoulos et al., 2025).

In humans, *MMP13* is expressed in the chondrocytes, epithelial and neuronal cells, connective tissues, and T lymphocytes. Under normal conditions, the expression of *MMP13* in humans is highly localized and upregulated in various diseases, such as artery and bone diseases (Hashimoto et al., 2013).

In zebrafish, *mmp13a* is expressed in the heart myocardium, macrophages, fin epidermis, and visceral epidermis, and *mmp13b* is expressed in the posterior cardinal vein and caudal fin (Sur et al., 2023). During zebrafish embryogenesis, the *mmp13a* paralogue plays an important role in hatching, while *mmp13b* is crucial for fin bone formation (Angelakopoulos et al., 2025).

MMP13 is a zinc-dependent proteolytic enzyme that is also known as collagenase 3. The most abundant protein in the extracellular matrix (ECM) is collagen, and essential biological processes such as tissue remodeling and angiogenesis depend on the collagenolytic activity of enzymes, such as MMP13. ECM is composed of a complex network of macromolecules such as proteins, glycoproteins, and proteoglycans and provides structural stability to the cells and facilitates cell adhesion and migration by functioning as a scaffold (Angelakopoulos et al., 2025). During heart failure, pathological remodeling and fibrosis of the heart lead to impaired cardiac function. The imbalance between the production and degradation of ECM is responsible for cardiac fibrosis. In response to injury, the cardiac fibroblasts secrete an excess amount of ECM proteins such as MMP13. Improvement in cardiac function is also observed after cardiac injury in mice treated with an MMP13 inhibitor (Schafer, 2018).

Unlike mammals, zebrafish can regenerate its heart after hypoxic injury primarily due to the ability of remaining cardiomyocytes to dedifferentiate and proliferate. In both zebrafish and mammals, collagenolytic activity is observed in the cardiac wall where collagen is deposited, leading to myocardial remodeling. Unlike mammals, the mechanical load of zebrafish hearts is decreased during the regeneration of myocardium, which leads to less collagen deposition. As the balance between the production and degradation of ECM shifts toward degradation, the collagen-rich scar is eventually reserved (Gamba et al., 2017).

During the inflammation phase after heart injury, MMPs (such as MMP13 and MMP9)-mediated leukocyte recruitment is essential for zebrafish heart regeneration, and inhibition of MMP13 is associated with reduced leukocyte recruitment and heart regeneration (Xu et al., 2018). The regeneration process of zebrafish hearts is associated with pro-regenerative macrophage activity, and the elimination of macrophages is linked to impaired myocardial regeneration. In neonatal mice and pigs, a similar myocardium regeneration capacity is observed, however this capacity is transient and lost in adults (Galili & Schaer, 2026).

However, an excessive inflammatory response was also found to be associated with impaired heart regeneration through decreased fibrotic scar degradation in *bre* mutant zebrafish hearts after cryoinjury, and a moderate dose of an MMP13/MMP9 inhibitor increased scar degradation by attenuating the inflammatory response. While the inflammatory response is essential for heart regeneration, excessive inflammation can have detrimental effects (Xu et al., 2019). This phenomenon might explain the decrease in fractional shortening (FS%) in the *mmp13a* and *mmp13b* knockout zebrafish, as opposed to the improved FS% observed in the previous study (Huttunen et al., 2024) using an MMP13 inhibitor.

Conclusion

In this study, an improvement in fractioning shortening (FS%) of the zebrafish embryo heart was observed in response to 60 minutes of hypoxia exposure in the CRISPR/Cas9-mediated *slc5a1* and *slc5a2* knockout embryos, whereas in the *mmp13b* knockout embryos, the fractioning shortening (FS%) was decreased after 45 minutes of hypoxia exposure. The improvement in FS% in the *slc5a1* and *slc5a2* knockout embryos might be the results of decreased intracellular Na^+ levels and improvement of cardiac energy supply by the formation of ketone bodies. This study also indicates that, while the overexpression of *mmp13a* and *mmp13b* is associated with the impaired heart regeneration capacity of zebrafish, knocking out the genes also impairs heart regeneration, suggesting a dose-dependent role of *mmp13a/mmp13b* inhibition in zebrafish heart regeneration.

4. Materials and methods

CRISPR design & primer selection

Four genes (*slc5a1, slc5a2, mmp13a,* and *mmp13b*) were selected for knockout using CRISPR/Cas9 in this study based on a previous study (Huttunen et al., 2024) conducted at the Zebrafish Core, Turku Bioscience. Two crRNAs (Table 3) were selected for each gene target using the online tool CHOPCHOP (https://chopchop.cbu.uib.no/) for *Danio rerio* (GRCz11/danRer11). The genome assembly GRCz11/danRer11 was released in 2017, and the total volume of data is 1.3 GB and contains 1917 scaffolds from assembling 19,725 contigs. The assembly was produced through combining fast DNA reading techniques with a detailed genetic map and DNA samples from the Tübingen (TU) fish strain (Okendo et al., 2025). While selecting the crRNA, it was ensured that both target sites were on the same exon for each of the target genes. For primer design, the PCR product size option was set from 300 to 500 base pairs, and the rest of the options were kept as defaults.

Two pairs of primers (Table 4 & Table 5) were selected for the nested PCR protocol. A nested PCR protocol is used to increase the sensitivity and specificity of the PCR. Nested PCR utilizes two different pairs of primers in two separate PCR steps, and the PCR product from the first amplification reaction is used as a template for the second PCR (Mr & J, 2019). In the first PCR, the amplification is performed with outer primer sets, and in the second PCR the inner primer sets anneal to an internal sequence of the first PCR (Khaksar et al., 2026).

Table 3. crRNA target sequences for CRISPR/Cas9 knockout

Target gene	**crRNA1**	**crRNA2**
slc5a1	TGGCCGGCAGAAGTATGGTGTGG	CGGACCAATCGAGCCACGGTCGG
slc5a2	ACTAATCGTGGCACAGTAGGCGG	CAGGTCGGACGATGGTGTGGTGG
mmp13a	CTCTAGGTCTAGGACACTCGCGG	ATGGGCCGCCACCGAGAACAGGG
mmp13b	CCGGGTACATAAGAGATCCAGGG	CTTTGGCGTAGGAGTAAACCGGG

Table 4. Outer forward and reverse primer sequences

Target gene	Outer forward	Outer reverse
slc5a1	cttcatacgaaaaagtttgggc	TAGGTTTATGGCCATTCTGGTC
slc5a2	TCAAATGCGGTATGAAAAACAC	CCCACCTATGTTGGGAAAATAA
mmp13a	CTTGACCAACGCACAAAATAAA	TTTTGAATCATCGGTATTGACG
mmp13b	cacacacacacacacacaaa	TCAGAATGGTGTATTGCTCACC

Table 5. Inner forward and reverse primer sequences

Target gene	Inner forward	Inner reverse
slc5a1	cttcatacgaaaaagtttgggc	GCCATTCTGGTCATTTTCTAGC
slc5a2	AAAAACACTTTGCCTCATCCAT	TTATACTCACAGGCCACCACAC
mmp13a	CATCGGTATTGACGTCAGTGTT	AACGCACAAAATAAAACCCAAC
mmp13b	tattagccccttctgtgcaaat	TGCTCACCATAGAGAGACTGGA

The *slc45a2* gene was also knocked out alongside each of the target genes. The crRNA sequences for the *slc45a2* gene target were GGTTTGGGAACCGGTCTGAT (ID: ZDB-CRISPR-150312-1) and GGCCATCGTGGTGGTGATGTT (ID: ZDB-CRISPR-151027-2).

The crRNAs (2 nmol), Alt-R™ *S.p.* Cas9 Nuclease V3 (62 µM), Alt-R™ CRISPR-Cas9 tracrRNA (5 nmol), and Alt-R™ CRISPR-Cas9 Negative Control crRNA #1 (2 nmol) were purchased from Integrated DNA Technologies (IDT), Inc.

crRNA:tracrRNA duplex preparation

The target crRNAs and negative control crRNA were dissolved in 20 µl of duplex buffer (IDT), and the tracrRNA was dissolved in 50 µl of duplex buffer, to a final concentration of 100 µM. Subsequently, 5 µl of tracrRNA and 2.5 µl of each of the two target crRNAs of the specific

gene were combined to form a 50 µM complex. For the negative control, 5 µl of negative control crRNA was combined with 5 µl of tracrRNA. 0.5 ml Eppendorf tubes were used to prepare the duplexes. The duplexes were prepared using a Bio-Rad S1000 Thermal Cycler. The protocol (Table 6) for the duplex preparation started with a denaturation step for 5 minutes at 95°C followed by cooling at a 0.1°C/sec ramp to 25°C and holding at 25°C for 5 minutes. Finally, it was cooled down and held at 4°C until the Eppendorf tubes were removed from the Bio-Rad S1000 Thermal Cycler.

Table 6. Thermal cycler protocol for crRNA:tracrRNA duplex preparation

Step	Temperature (°C)	Duration
Denaturation	95°C	5 minutes
Cooling	0.1°C/sec ramp	Until 25°C
Hold	25°C	5 minutes
Final hold	4°C	∞

Subsequently, 10 µl of duplex buffer was added to achieve a final concentration of 25 µM and a final volume of 20 µl. The duplexes were prepared in advance and stored at −20°C.

Fish mating and embryo collection

The wild-type (AB) zebrafish strain was used in this study. Fish matings were set up in the afternoon prior to microinjection the following morning. The matings were set up with a divider to ensure that no mating occurred during the night or early morning. The divider was removed at approximately 08:30, and the fish were allowed to mate for 20–30 minutes. The early-stage embryos were then collected and maintained in an 18°C incubator to slow down their development prior to microinjection.

Cas9 RNP complex preparation

The Cas9 ribonucleoprotein (RNP) complex was prepared before the microinjection in the morning after collecting the zebrafish embryos. The components were mixed according to the protocol (Table 7) in an 0.5 Eppendorf tube and kept on ice.

Table 7. Components and volume of the Cas9 RNP complex

Component	**Negative control (µl)**	**Target (µl)**
Negative control duplex (25 uM)	0.5	
slc45a2 duplex (25 uM)	0.5	0.5
Target duplex (25 uM)		0.5
IDT Cas9 nuclease (62 µM)	0.4	0.4
KCL, 3M	0.4	0.4
Phenol red	1.0	1.0
Nuclease-free water (IDT)	2.2	2.2

Microinjection

A vertical needle-pulling instrument (Narishige PB-7) was used to produce the microinjection needles. A Nanoject II Auto-Nanoliter Injector (3-000-205A, Drummond) was used to inject 2.3 nL of Cas9 RNP complex into early-stage zebrafish embryos (1- to 4-cell stages). The embryos were aligned against a glass slide on a petri dish lid, and excess liquid was removed to ensure that the embryos were fixed in position for microinjection. The entire procedure was performed under a stereo microscope.

Following microinjection, the embryos were gently washed into a petri dish containing E3 medium (5 mM NaCl, 0.17 mM KCl, 0.33 mM $CaCl_2$, 0.33 mM $MgSO_4$) supplemented with 1:200 Pen-Strep and maintained in a 28°C incubator to recover and develop.

Exposure to hypoxia

At three days post-fertilization (3 dpf), the injected embryos, along with the negative controls, were exposed to hypoxia. The hypoxia solution was prepared by dissolving sodium metabisulfite in E3 medium (1 mg/mL). The pH of the hypoxia solution was adjusted with KOH to pH 6.8–7.0. The solution was then equilibrated in a 28.5°C incubator prior to use.

The embryos were anesthetized with Tricaine (MS-222; 200 mg/L) prior to exposure to hypoxia. The embryos were then exposed to hypoxic conditions for 45 minutes in the first experiment and 60 minutes in the second experiment, in a 30 mL glass vial maintained inside a 28.5°C incubator. Following exposure, the embryos were removed from the hypoxia solution and transferred into a Petri dish containing E3 medium. The embryos were subsequently maintained in a 28.5°C incubator overnight to recover, and imaging was performed the following day.

Imaging and image analysis

At four days post-fertilization (4 dpf), cardiac imaging of the embryos was performed using a Nikon Eclipse Ti2-E microscope. The embryos were anesthetized with tricaine (MS-222; 200 mg/L) and placed into a 96-well plate.

A short cardiac video (5–10 seconds) from each embryo was recorded using a Plan Fluor 10x/0.30 OFN25 Ph1 DL (MRH20101) lens at 100 frames per second (FPS), and the videos were analyzed using ImageJ/Fiji. From the heart recordings, the dimensions of the zebrafish heart at diastole (maximum length at the end of the relaxation phase) and systole (minimum length following the contraction phase) were measured. The fractional shortening (FS%) was subsequently calculated using the following formula:

$$FS\% = \frac{Diastolic\ length - Systolic\ length}{Diastolic\ length} \times 100\%$$

DNA extraction

DNA was extracted using the HotShot method (Meeker et al., 2007). The embryos were collected in 1.5 mL Eppendorf tubes. A volume of 50 µL of 50 mM NaOH per embryo was

added to the tube and incubated at 95°C for 20 minutes. Once the embryos were completely dissolved, the tubes were cooled on ice, and 5.5 µL of 1M Tris-HCl (pH 8.0) per embryo was added to neutralize the NaOH. The samples were then vortexed and centrifuged at maximum speed for 5 minutes. The resulting supernatant was used for PCR.

PCR and agarose gel electrophoresis

PCR was carried out using a nested PCR protocol (Table 8). For the first PCR reaction, 19.5 µL of PCR-grade water, 25 µL of KOD One™ PCR Master Mix (Japan), 1.5 µL of outer forward primer (10 µM), and 1.5 µL of outer reverse primer (10 µM) were combined, and 9.5 µL of the mixture was distributed into 0.5 mL Eppendorf tubes. A volume of 0.5 µL of DNA extract was added to individual tubes. Milli-Q® water (0.5 µL) was included as a negative control. PCR was performed using a Bio-Rad S1000 Thermal Cycler with the following protocol:

Table 8. Nested PCR thermal cycler protocol

Step	Temperature (°C)	Time (sec)
Denaturation	98.0	10
Annealing (TM -5 °C)	55.0	5
Extension	68.0	1
Cycle, 30x		
Hold	4	Infinite

For the second PCR reaction, 1.5 µL of inner forward primer (10 µM) and 1.5 µL of inner reverse primer (10 µM) were combined with 19.5 µL of PCR-grade water and 25 µL of KOD One™ PCR Master Mix. A volume of 9.5 µL of the mixture was distributed into 0.5 mL Eppendorf tubes, and 0.5 µL of the first PCR product was added to each tube. The second PCR was carried out using the same protocol as the first PCR reaction.

The second PCR product was verified by agarose gel electrophoresis. For gel preparation, 1 g of agarose was measured into an Erlenmeyer flask, and 50 mL of 1× TAE (Tris-acetate EDTA) buffer was added to prepare a 2.0% gel. The mixture was heated in a microwave oven

until a uniform solution was obtained. The solution was cooled to approximately 60°C, and 5 µL of SYBR™ Safe DNA Gel Stain (1:10,000; Invitrogen™) was added to the agarose solution.

The gel cassette was assembled by taping the ends and placing it on a flat surface. The agarose solution was poured into the cassette, and a sample comb was inserted. Once fully solidified, the comb was removed and the cassette was placed in an electrophoresis chamber filled with 1× TAE buffer, ensuring that the gel was fully submerged. A volume of 5 µL of MassRuler DNA Ladder (Thermo Scientific™) was loaded into the first and last wells, and the second PCR products were loaded into the intervening wells. The gel was run at 90 V for approximately one hour and visualized using a Bio-Rad Gel Doc XR+ Gel Documentation System.

PCR product purification

The PCR products were purified using the Monarch® PCR & DNA Cleanup Kit (New England Biolabs Inc.) or with the Agarose Gel DNA Extraction Kit (Roche, Version 13), according to the instruction provided by the manufacturer. The NanoDrop Lite Spectrophotometer (Thermo Fisher Scientific) was used to measure the concentration of the purified DNA.

Sanger sequencing and TIDE analysis

Sanger sequencing was performed using the LightRun sequencing service (Eurofins Genomics). LightRun tube samples were prepared by combining 5 µL of purified PCR product (5 ng/µL) with 5 µL of primer (5 µM).

Editing efficacy was quantified from the resulting chromatograms using the Tracking of Indels by Decomposition (TIDE) (Brinkman et al., 2014) software (https://apps.datacurators.nl/tide/) by uploading the .ab1 files of the target gene-edited samples and the corresponding control samples. All parameters within the TIDE software were kept at their default settings.

Statistical analysis

Statistical analyses were performed using R version 4.5.1 (2025-06-13) and the numiqo statistics calculator (https://numiqo.com/). The normality of the data was assessed using the Shapiro-Wilk test, in addition to visual inspection of histograms and Q-Q plots. If the data were found to be normally distributed, Levene's test was performed to assess the homogeneity of variances; if the data were not normally distributed, the Kruskal-Wallis test was performed. If the variances were found to be equal, a one-way ANOVA was performed; if the variances were not equal, Welch's test was performed, followed by Dunnett's post-hoc test to compare each experimental group against the control group. A p-value of less than 0.05 was considered statistically significant. Data are presented as box plots with individual data points overlaid, generated using the numiqo statistics calculator (https://numiqo.com/).

5. Abbreviations

AMI	Acute myocardial infarction
ACEIs	Angiotensin-converting enzyme inhibitors
ACS	Acute coronary syndrome
aEPC	Activated epithelial progenitor cells
Ang II	Angiotensin II
ARBs	Angiotensin II receptor blockers
ARNIs	Angiotensin receptor neprilysin inhibitors
BNP	Brain natriuretic peptide
CAD	Coronary artery disease
CKD	Chronic kidney disease
CMR	Cardiac magnetic resonance
CRISPR	Clustered regularly interspaced short palindromic repeats
crRNAs	CRISPR RNAs
CTA	Computed tomography angiography
dpf	Days post fertilization
ECG	Electrocardiography
ECM	Extracellular matrix
EF	Ejection fraction
EMT	Epithelial mesenchymal transition
FFAs	Free fatty acids
FIH	Factor-inhibiting HIF
FS%	Fractional shortening
GLUT1	Glucose transporter-1
GLUT3	Glucose transporter-3
gRNAs	Guide RNAs
HF	Heart failure
HFimEF	Heart failure with improved ejection fraction
HFmrEF	Heart failure with mildly reduced ejection fraction
HFpEF	Heart failure with preserved ejection fraction
HFrEF	Heart failure with reduced ejection fraction
HIF-α	Hypoxia-inducible factor α
HRE	Hypoxia response element
ICAM-1	Intercellular adhesion molecule 1
IL-1β	Interleukin-1 beta
IL-6	Interleukin-6
LDL-C	low-density lipoprotein cholesterol

LV	Left ventricle
LVEF	Left ventricular ejection fraction
LVH	Left ventricular hypertrophy
MI	Myocardial infarction
mmp13a	Matrix metalloproteinase 13a
mmp13b	Matrix metalloproteinase 13b
MRAs	Mineralocorticoid receptor antagonists
NHE1	Na^+/H^+ exchanger 1
NHE3	Na^+/H^+ exchanger 3
NO	Nitric oxide
NOSs	NO synthases
NT-proBNP	N-terminal pro-BNP
PHDs	Prolyl hydroxylase domain-containing proteins
pVHL	von Hippel-Lindau tumor suppressor
QoL	Quality of life
RAAS	Renin-angiotensin-aldosterone system
ROS	Reactive oxygen species
SGLT1	Sodium glucose co-transporter 1
SGLT2	Sodium glucose co-transporter 2
SGLT2i	Sodium-glucose cotransporter 2 inhibitors
slc5a1	Solute carrier family 5-member 1
slc5a2	Solute carrier family 5-member 2
TALENs	Transcription activator-like effector nucleases
TIDE	Tracking of indels by decomposition
VEGF	Vascular endothelial growth factor
VHD	Valvular heart disease
WGD	Whole genome duplication
ZFNs	Zinc finger nucleases

6. References

Al-Shamasi, A.-A., Elkaffash, R., Mohamed, M., Rayan, M., Al-Khater, D., Gadeau, A.-P., Ahmed, R., Hasan, A., Eldassouki, H., Yalcin, H. C., Abdul-Ghani, M., & Mraiche, F. (2021). Crosstalk between Sodium–Glucose Cotransporter Inhibitors and Sodium–Hydrogen Exchanger 1 and 3 in Cardiometabolic Diseases. *International Journal of Molecular Sciences*, *22*(23), 12677. https://doi.org/10.3390/ijms222312677

Angelakopoulos, R., Tsipourlianos, A., Maravelakis, I. D., Giannoulis, T., Mamuris, Z., & Moutou, K. A. (2025). Evolutionary Dynamics of Matrix Metalloproteases with Collagenolytic Activity in Teleosts. *Animals : An Open Access Journal from MDPI*, *15*(22), 3270. https://doi.org/10.3390/ani15223270

Angom, R. S., & Nakka, N. M. R. (2024). Zebrafish as a Model for Cardiovascular and Metabolic Disease: The Future of Precision Medicine. *Biomedicines*, *12*(3), 693. https://doi.org/10.3390/biomedicines12030693

Angom, R. S., Singh, M., Muhammad, H., Varanasi, S. M., & Mukhopadhyay, D. (2025). Zebrafish as a Versatile Model for Cardiovascular Research: Peering into the Heart of the Matter. *Cells*, *14*(7), 531. https://doi.org/10.3390/cells14070531

Apolínová, K., Pérez, F. A., Dyballa, S., Coppe, B., Mercader Huber, N., Terriente, J., & Di Donato, V. (2024). ZebraReg—A novel platform for discovering regulators of cardiac regeneration using zebrafish. *Frontiers in Cell and Developmental Biology*, *12*. https://doi.org/10.3389/fcell.2024.1384423

Aziz, W., Claridge, S., Ntalas, I., Gould, J., de Vecchi, A., Razeghi, O., Toth, D., Mountney, P., Preston, R., Rinaldi, C. A., Razavi, R., Niederer, S., & Rajani, R. (2019). Emerging role

of cardiac computed tomography in heart failure. *ESC Heart Failure*, *6*(5), 909–920. https://doi.org/10.1002/ehf2.12479

Basuray, A., Dolansky, M., Josephson, R., Sattar, A., Grady, E. M., Vehovec, A., Gunstad, J., Redle, J., Fang, J., & Hughes, J. W. (2015). Dietary Sodium Adherence Is Poor in Chronic Heart Failure Patients. *Journal of Cardiac Failure*, *21*(4), 323–329. https://doi.org/10.1016/j.cardfail.2014.12.016

Begeman, I. J., & Kang, J. (2018). Transcriptional Programs and Regeneration Enhancers Underlying Heart Regeneration. *Journal of Cardiovascular Development and Disease*, *6*(1), 2. https://doi.org/10.3390/jcdd6010002

Biegus, J., Niewinski, P., Josiak, K., Kulej, K., Ponikowska, B., Nowak, K., Zymlinski, R., & Ponikowski, P. (2021). Pathophysiology of Advanced Heart Failure: What Knowledge Is Needed for Clinical Management? *Heart Failure Clinics, Advanced Heart Failure: From Pathophysiology to Clinical Management*, *17*(4), 519–531. https://doi.org/10.1016/j.hfc.2021.06.001

Bowley, G., Kugler, E., Wilkinson, R., Lawrie, A., Eeden, F. van, Chico, T. J. A., Evans, P. C., Noël, E. S., & Serbanovic-Canic, J. (2022). Zebrafish as a tractable model of human cardiovascular disease. *British Journal of Pharmacology*, *179*(5), 900–917. https://doi.org/10.1111/bph.15473

Bradford, Y. M., Van Slyke, C. E., Ruzicka, L., Singer, A., Eagle, A., Fashena, D., Howe, D. G., Frazer, K., Martin, R., Paddock, H., Pich, C., Ramachandran, S., & Westerfield, M. (2022). Zebrafish information network, the knowledgebase for Danio rerio research. *Genetics*, *220*(4), iyac016. https://doi.org/10.1093/genetics/iyac016

Brinkman, E. K., Chen, T., Amendola, M., & van Steensel, B. (2014). Easy quantitative assessment of genome editing by sequence trace decomposition. *Nucleic Acids Research*, *42*(22), e168. https://doi.org/10.1093/nar/gku936

Brociek, E., Tymińska, A., Giordani, A. S., Caforio, A. L. P., Wojnicz, R., Grabowski, M., & Ozierański, K. (2023). Myocarditis: Etiology, Pathogenesis, and Their Implications in Clinical Practice. *Biology*, *12*(6), 874. https://doi.org/10.3390/biology12060874

Burggren, W., Abramova, R., Bautista, N. M., Fritsche Danielson, R., Dubansky, B., Gupta, A., Hansson, K., Iyer, N., Jagadeeswaran, P., Jennbacken, K., Rydén-Markinhutha, K., Patel, V., Raman, R., Trivedi, H., Vazquez Roman, K., Williams, S., & Wang, Q.-D. (2024). A larval zebrafish model of cardiac physiological recovery following cardiac arrest and myocardial hypoxic damage. *Biology Open*, *13*(9), bio060230. https://doi.org/10.1242/bio.060230

Cai, X., Zhang, D., Wang, J., Liu, X., Ouyang, G., & Xiao, W. (2018). Deletion of the fih gene encoding an inhibitor of hypoxia-inducible factors increases hypoxia tolerance in zebrafish. *The Journal of Biological Chemistry*, *293*(40), 15370–15380. https://doi.org/10.1074/jbc.RA118.003004

Cerra, M. C., Filice, M., Caferro, A., Mazza, R., Gattuso, A., & Imbrogno, S. (2023). Cardiac Hypoxia Tolerance in Fish: From Functional Responses to Cell Signals. *International Journal of Molecular Sciences*, *24*(2), 1460. https://doi.org/10.3390/ijms24021460

Cesare, M. D., Perel, P., Taylor, S., Kabudula, C., Bixby, H., Gaziano, T. A., McGhie, D. V., Mwangi, J., Pervan, B., Narula, J., Pineiro, D., & Pinto, F. J. (2024). The Heart of the World. *Global Heart*, *19*(1). https://doi.org/10.5334/gh.1288

Chen, S., Wang, Q., Bakker, D., Hu, X., Zhang, L., van der Made, I., Tebbens, A. M., Kovácsházi, C., Giricz, Z., Brenner, G. B., Ferdinandy, P., Schaart, G., Gemmink, A., Hesselink, M. K. C., Rivaud, M. R., Pieper, M. P., Hollmann, M. W., Weber, N. C., Balligand, J.-L., … Zuurbier, C. J. (2024). Empagliflozin prevents heart failure through inhibition of the NHE1-NO pathway, independent of SGLT2. *Basic Research in Cardiology*, *119*(5), 751–772. https://doi.org/10.1007/s00395-024-01067-9

Chen, S., Wang, Q., Christodoulou, A., Mylonas, N., Bakker, D., Nederlof, R., Hollmann, M. W., Weber, N. C., Coronel, R., Wakker, V., Christoffels, V. M., Andreadou, I., & Zuurbier, C. J. (2023). Sodium Glucose Cotransporter-2 Inhibitor Empagliflozin Reduces Infarct Size Independently of Sodium Glucose Cotransporter-2. *Circulation*, *147*(3), 276–279. https://doi.org/10.1161/CIRCULATIONAHA.122.061688

Cholesterol Treatment Trialists' (Ctt) Collaboration. (2010). Efficacy and safety of more intensive lowering of LDL cholesterol: A meta-analysis of data from 170 000 participants in 26 randomised trials. *The Lancet*, *376*(9753), 1670–1681. https://doi.org/10.1016/S0140-6736(10)61350-5

Cohn, J. N., Ferrari, R., & Sharpe, N. (2000). Cardiac remodeling—concepts and clinical implications: A consensus paper from an international forum on cardiac remodeling. *Journal of the American College of Cardiology*, *35*(3), 569–582. https://doi.org/10.1016/S0735-1097(99)00630-0

Dini, F. L., Cameli, M., Stefanini, A., Aboumarie, H. S., Lisi, M., Lindqvist, P., & Henein, M. Y. (2024). Echocardiography in the Assessment of Heart Failure Patients. *Diagnostics*, *14*(23), 2730. https://doi.org/10.3390/diagnostics14232730

Ekanayake, P., Hupfeld, C., & Mudaliar, S. (2020). Sodium-Glucose Cotransporter Type 2 (SGLT-2) Inhibitors and Ketogenesis: The Good and the Bad. *Current Diabetes Reports*, *20*(12), 74. https://doi.org/10.1007/s11892-020-01359-z

Elks, P. M., Renshaw, S. A., Meijer, A. H., Walmsley, S. R., & van Eeden, F. J. (2015). Exploring the HIFs, buts and maybes of hypoxia signalling in disease: Lessons from zebrafish models. *Disease Models & Mechanisms*, *8*(11), 1349–1360. https://doi.org/10.1242/dmm.021865

Epperson, J., Athar, Z. M., Arshad, M., & Chen, E. (2024). A Review of Sodium-Glucose Cotransporter 2 Inhibitor's Clinical Efficacy in Heart Failure With Preserved Ejection Fraction. *Cureus*, *16*(4), e57380. https://doi.org/10.7759/cureus.57380

Ezekowitz, J. A., Colin-Ramirez, E., Ross, H., Escobedo, J., Macdonald, P., Troughton, R., Saldarriaga, C., Alemayehu, W., McAlister, F. A., Arcand, J., Atherton, J., Doughty, R., Gupta, M., Howlett, J., Jaffer, S., Lavoie, A., Lund, M., Marwick, T., McKelvie, R., … Zieroth, S. (2022). Reduction of dietary sodium to less than 100 mmol in heart failure (SODIUM-HF): An international, open-label, randomised, controlled trial. *The Lancet*, *399*(10333), 1391–1400. https://doi.org/10.1016/S0140-6736(22)00369-5

Farzam, K., & Jan, A. (2026). Beta Blockers. In *StatPearls*. StatPearls Publishing. http://www.ncbi.nlm.nih.gov/books/NBK532906/

Galili, U., & Schaer, G. L. (2026). Lessons of Macrophage-Associated Heart Regeneration in Fish, Amphibians, and Neonatal Mice, Applied to Adult Mice: A Perspective on α-Gal Nanoparticles. *International Journal of Molecular Sciences*, *27*(4), 1950. https://doi.org/10.3390/ijms27041950

Gamba, L., Amin-Javaheri, A., Kim, J., Warburton, D., & Lien, C.-L. (2017). Collagenolytic Activity Is Associated with Scar Resolution in Zebrafish Hearts after Cryoinjury. *Journal of Cardiovascular Development and Disease*, *4*(1), 2. https://doi.org/10.3390/jcdd4010002

García-Ropero, Á., Vargas-Delgado, A. P., Santos-Gallego, C. G., & Badimon, J. J. (2019). Inhibition of Sodium Glucose Cotransporters Improves Cardiac Performance. *International Journal of Molecular Sciences*, *20*(13), 3289. https://doi.org/10.3390/ijms20133289

Gerber, Y., Rosen, L. J., Goldbourt, U., Benyamini, Y., Drory, Y., & Israel Study Group on First Acute Myocardial Infarction. (2009). Smoking Status and Long-Term Survival After First Acute Myocardial Infarction. *JACC*, *54*(25), 2382–2387. https://doi.org/10.1016/j.jacc.2009.09.020

GHERASIM, L. (2019). Troponins in Heart Failure – a Perpetual Challenge. *Mædica*, *14*(4), 371–377. https://doi.org/10.26574/maedica.2019.14.4.371

Golla, M. S. G., Hajouli, S., & Ludhwani, D. (2026). Heart Failure and Ejection Fraction. In *StatPearls*. StatPearls Publishing. http://www.ncbi.nlm.nih.gov/books/NBK553115/

González-Rosa, J. M., Sharpe, M., Field, D., Soonpaa, M. H., Field, L. J., Burns, C. E., & Burns, C. G. (2018). Myocardial polyploidization creates a barrier to heart

regeneration in zebrafish. *Developmental Cell*, *44*(4), 433-446.e7. https://doi.org/10.1016/j.devcel.2018.01.021

Greenald, D., Jeyakani, J., Pelster, B., Sealy, I., Mathavan, S., & van Eeden, F. J. (2015). Genome-wide mapping of Hif-1α binding sites in zebrafish. *BMC Genomics*, *16*, 923. https://doi.org/10.1186/s12864-015-2169-x

Grundy, S. M., Stone, N. J., Bailey, A. L., Beam, C., Birtcher, K. K., Blumenthal, R. S., Braun, L. T., de Ferranti, S., Faiella-Tommasino, J., Forman, D. E., Goldberg, R., Heidenreich, P. A., Hlatky, M. A., Jones, D. W., Lloyd-Jones, D., Lopez-Pajares, N., Ndumele, C. E., Orringer, C. E., Peralta, C. A., … Yeboah, J. (2019). 2018 AHA/ACC/AACVPR/AAPA/ABC/ACPM/ADA/AGS/APhA/ASPC/NLA/PCNA Guideline on the Management of Blood Cholesterol: A Report of the American College of Cardiology/American Heart Association Task Force on Clinical Practice Guidelines. *Circulation*, *139*(25), e1082–e1143. https://doi.org/10.1161/CIR.0000000000000625

Gyimesi, G., Pujol-Giménez, J., Kanai, Y., & Hediger, M. A. (2020). Sodium-coupled glucose transport, the SLC5 family, and therapeutically relevant inhibitors: From molecular discovery to clinical application. *Pflugers Archiv*, *472*(9), 1177–1206. https://doi.org/10.1007/s00424-020-02433-x

Hashimoto, K., Otero, M., Imagawa, K., de Andrés, M. C., Coico, J. M., Roach, H. I., Oreffo, R. O. C., Marcu, K. B., & Goldring, M. B. (2013). Regulated Transcription of Human Matrix Metalloproteinase 13 (MMP13) and Interleukin-1β (IL1B) Genes in Chondrocytes Depends on Methylation of Specific Proximal Promoter CpG Sites.

The Journal of Biological Chemistry, *288*(14), 10061–10072. https://doi.org/10.1074/jbc.M112.421156

He, Y., Huang, C.-X., Chen, N., Wu, M., Huang, Y., Liu, H., Tang, R., Wang, W.-M., & Wang, H.-L. (2017). The zebrafish miR-125c is induced under hypoxic stress via hypoxia-inducible factor 1α and functions in cellular adaptations and embryogenesis. *Oncotarget*, *8*(43), 73846–73859. https://doi.org/10.18632/oncotarget.17994

Herman, L. L., Padala, S. A., Ahmed, I., & Bashir, K. (2026). Angiotensin-Converting Enzyme Inhibitors (ACEI). In *StatPearls*. StatPearls Publishing. http://www.ncbi.nlm.nih.gov/books/NBK431051/

Hoareau, M., El Kholti, N., Debret, R., & Lambert, E. (2022). Zebrafish as a Model to Study Vascular Elastic Fibers and Associated Pathologies. *International Journal of Molecular Sciences*, *23*(4), 2102. https://doi.org/10.3390/ijms23042102

Hu, B., Lelek, S., Spanjaard, B., El-Sammak, H., Simões, M. G., Mintcheva, J., Aliee, H., Schäfer, R., Meyer, A. M., Theis, F., Stainier, D. Y. R., Panáková, D., & Junker, J. P. (2022). Origin and function of activated fibroblast states during zebrafish heart regeneration. *Nature Genetics*, *54*(8), 1227–1237. https://doi.org/10.1038/s41588-022-01129-5

Huttunen, R., Haapanen-Saaristo, A.-M., Hjelt, A., Jokilammi, A., Paatero, I., & Järveläinen, H. (2024). Empagliflozin attenuates hypoxia-induced heart failure of zebrafish embryos via influencing MMP13 expression. *Biomedicine & Pharmacotherapy*, *180*, 117453. https://doi.org/10.1016/j.biopha.2024.117453

Huusko, J., Kurki, S., Toppila, I., Purmonen, T., Lassenius, M., Gullberg, E., Wirta, S. B., & Ukkonen, H. (2019). Heart failure in Finland: Clinical characteristics, mortality, and healthcare resource use. *ESC Heart Failure*, *6*(4), 603–612. https://doi.org/10.1002/ehf2.12443

Hwang, W. Y., Fu, Y., Reyon, D., Maeder, M. L., Tsai, S. Q., Sander, J. D., Peterson, R. T., Yeh, J.-R. J., & Joung, J. K. (2013). Efficient genome editing in zebrafish using a CRISPR-Cas system. *Nature Biotechnology*, *31*(3), 227–229. https://doi.org/10.1038/nbt.2501

Ibsen, D. B., Levitan, E. B., Åkesson, A., Gigante, B., & Wolk, A. (2022). The DASH diet is associated with a lower risk of heart failure: A cohort study. *European Journal of Preventive Cardiology*, *29*(7), 1114–1123. https://doi.org/10.1093/eurjpc/zwac003

Jao, L.-E., Wente, S. R., & Chen, W. (2013). Efficient multiplex biallelic zebrafish genome editing using a CRISPR nuclease system. *Proceedings of the National Academy of Sciences*, *110*(34), 13904–13909. https://doi.org/10.1073/pnas.1308335110

Jopling, C., Suñé, G., Faucherre, A., Fabregat, C., & Izpisua Belmonte, J. C. (2012). Hypoxia Induces Myocardial Regeneration in Zebrafish. *Circulation*, *126*(25), 3017–3027. https://doi.org/10.1161/CIRCULATIONAHA.112.107888

Jugdutt, B. I. (2012). Ischemia/Infarction. *Heart Failure Clinics*, *8*(1), 43–51. https://doi.org/10.1016/j.hfc.2011.08.006

Kantor, A., McClements, M. E., & MacLaren, R. E. (2020). CRISPR-Cas9 DNA Base-Editing and Prime-Editing. *International Journal of Molecular Sciences*, *21*(17), 6240. https://doi.org/10.3390/ijms21176240

Kemp, C. D., & Conte, J. V. (2012). The pathophysiology of heart failure. *Cardiovascular Pathology*, *21*(5), 365–371. https://doi.org/10.1016/j.carpath.2011.11.007

Khaksar, S., Latifi, A., Mohebali, M., Atighehchian, M., Moradian, A., Asadigandomani, H., Rezaian, M., Anasori, N., Koosha, M., Pellegrino, K., Izadi, S., Goudarzi, F., Kazemirad, E., & Soleimani, M. (2026). Nested PCR as a superior diagnostic method for Acanthamoeba keratitis compared to conventional techniques. *Scientific Reports*, *16*(1), 3502. https://doi.org/10.1038/s41598-025-32716-1

Khan, M. G. (2015). Angiotensin-Converting Enzyme Inhibitors and Angiotensin II Receptor Blockers. In M. G. Khan (Ed.), *Cardiac Drug Therapy* (pp. 85–127). Humana Press. https://doi.org/10.1007/978-1-61779-962-4_3

Khan, M. S., Fonarow, G. C., Ahmed, A., Greene, S. J., Vaduganathan, M., Khan, H., Marti, C., Gheorghiade, M., & Butler, J. (2017). Dose of Angiotensin-Converting Enzyme Inhibitors and Angiotensin Receptor Blockers and Outcomes in Heart Failure. *Circulation: Heart Failure*, *10*(8), e003956. https://doi.org/10.1161/CIRCHEARTFAILURE.117.003956

Kopp, R., Bauer, I., Ramalingam, A., Egg, M., & Schwerte, T. (2014). Prolonged Hypoxia Increases Survival Even in Zebrafish (Danio rerio) Showing Cardiac Arrhythmia. *PLoS ONE*, *9*(2), e89099. https://doi.org/10.1371/journal.pone.0089099

Kozman, K., Ferrannini, G., Benson, L., Dahlström, U., Hage, C., Savarese, G., Shahim, B., & Lund, L. H. (2025). Etiology of Heart Failure Across the Ejection Fraction Spectrum and Association With Prognosis. *JACC: Heart Failure*, *13*(8), 102491. https://doi.org/10.1016/j.jchf.2025.03.037

Lawrence, S. P., Holman, G. D., & Koumanov, F. (2010). Translocation of the Na+/H+ exchanger 1 (NHE1) in cardiomyocyte responses to insulin and energy-status signalling. *Biochemical Journal*, *432*(Pt 3), 515–523. https://doi.org/10.1042/BJ20100717

Liao, Q., Deng, H., Wang, Z., Yu, G., Zhu, C., Jia, S., Liu, W., Bai, Y., Sun, X., Chen, X., Xiao, W., & Liu, X. (2023). Deletion of prolyl hydroxylase domain-containing enzyme 3 (phd3) in zebrafish facilitates hypoxia tolerance. *The Journal of Biological Chemistry*, *299*(12), 105420. https://doi.org/10.1016/j.jbc.2023.105420

Lin, H., Guan, L., Meng, L., Uzui, H., & Guo, H. (2021). SGLT1 Knockdown Attenuates Cardiac Fibroblast Activation in Diabetic Cardiac Fibrosis. *Frontiers in Pharmacology*, *12*, 700366. https://doi.org/10.3389/fphar.2021.700366

Liu, C., Ferrari, V. A., & Han, Y. (2021). Cardiovascular Magnetic Resonance Imaging and Heart Failure. *Current Cardiology Reports*, *23*(4), 35. https://doi.org/10.1007/s11886-021-01464-9

Liu, H., Magaye, R., Kaye, D. M., & Wang, B. H. (2024a). Heart failure with preserved ejection fraction: The role of inflammation. *European Journal of Pharmacology*, *980*, 176858. https://doi.org/10.1016/j.ejphar.2024.176858

Liu, H., Magaye, R., Kaye, D. M., & Wang, B. H. (2024b). Heart failure with preserved ejection fraction: The role of inflammation. *European Journal of Pharmacology*, *980*, 176858. https://doi.org/10.1016/j.ejphar.2024.176858

Lopez-Usina, A., Mantilla-Cisneros, C., & Llerena-Velastegui, J. (2024). Comprehensive Benefits of Sodium-Glucose Cotransporter 2 Inhibitors in Heart Failure With

Reduced Ejection Fraction: A Literature Review. *Journal of Clinical Medicine Research*, *16*(10), 449–464. https://doi.org/10.14740/jocmr6033

Lovatt, S., Wong, C. W., Holroyd, E., Butler, R., Phan, T., Patwala, A., Loke, Y. K., Mallen, C. D., & Kwok, C. S. (2021). Smoking cessation after acute coronary syndrome: A systematic review and meta-analysis. *International Journal of Clinical Practice*, *75*(12), e14894. https://doi.org/10.1111/ijcp.14894

Lu, S., Hu, M., Wang, Z., Liu, H., Kou, Y., Lyu, Z., & Tian, J. (2020). Generation and Application of the Zebrafish heg1 Mutant as a Cardiovascular Disease Model. *Biomolecules*, *10*(11), 1542. https://doi.org/10.3390/biom10111542

Masarone, D., Martucci, M. L., Errigo, V., & Pacileo, G. (2021). The Use of β-Blockers in Heart Failure with Reduced Ejection Fraction. *Journal of Cardiovascular Development and Disease*, *8*(9), 101. https://doi.org/10.3390/jcdd8090101

McBeath, K., & Cowie, M. R. (2022a). Heart failure: Classification and pathophysiology. *Medicine*, *50*(8), 471–478. https://doi.org/10.1016/j.mpmed.2022.05.001

McBeath, K., & Cowie, M. R. (2022b). Heart failure: Classification and pathophysiology. *Medicine, Cardiovascular Medicine Part 3 of 4*, *50*(8), 471–478. https://doi.org/10.1016/j.mpmed.2022.05.001

Meeker, N. D., Hutchinson, S. A., Ho, L., & Trede, N. S. (2007). Method for Isolation of PCR-Ready Genomic DNA from Zebrafish Tissues. *BioTechniques*, *43*(5), 610–614. https://doi.org/10.2144/000112619

Moreno-Sánchez, I., Hernández-Huertas, L., Nahón-Cano, D., Martínez-García, P. M., Treichel, A. J., Gómez-Marin, C., Tomás-Gallardo, L., da Silva Pescador, G.,

Kushawah, G., Egidy, R., Perera, A., Díaz-Moscoso, A., Cano-Ruiz, A., Walker, J. A., Muñoz, M. J., Holden, K., Galcerán, J., Nieto, M. Á., Bazzini, A. A., & Moreno-Mateos, M. A. (2025). Enhanced RNA-targeting CRISPR-Cas technology in zebrafish. *Nature Communications*, *16*(1), 2591. https://doi.org/10.1038/s41467-025-57792-9

Mr, G., & J, S. (2019). Nested Polymerase Chain Reaction (PCR). *Cold Spring Harbor Protocols*, *2019*(2). https://doi.org/10.1101/pdb.prot095182

Murphy, S. P., Kakkar, R., McCarthy, C. P., & Januzzi, J. L. (2020). Inflammation in Heart Failure. *JACC*, *75*(11), 1324–1340. https://doi.org/10.1016/j.jacc.2020.01.014

Nappi, F. (2025). Myocarditis and Inflammatory Cardiomyopathy in Dilated Heart Failure. *Viruses*, *17*(4), 484. https://doi.org/10.3390/v17040484

Narumanchi, S., Wang, H., Perttunen, S., Tikkanen, I., Lakkisto, P., & Paavola, J. (2021). Zebrafish Heart Failure Models. *Frontiers in Cell and Developmental Biology*, *9*, 662583. https://doi.org/10.3389/fcell.2021.662583

Niriayo, Y. L., Asgedom, S. W., Demoz, G. T., & Gidey, K. (2020). Treatment optimization of beta-blockers in chronic heart failure therapy. *Scientific Reports*, *10*(1), 15903. https://doi.org/10.1038/s41598-020-72836-4

Nissen, S. E., Lincoff, A. M., Brennan, D., Ray, K. K., Mason, D., Kastelein, J. J. P., Thompson, P. D., Libby, P., Cho, L., Plutzky, J., Bays, H. E., Moriarty, P. M., Menon, V., Grobbee, D. E., Louie, M. J., Chen, C.-F., Li, N., Bloedon, L., Robinson, P., … CLEAR Outcomes Investigators. (2023). Bempedoic Acid and Cardiovascular Outcomes in Statin-Intolerant Patients. *The New England Journal of Medicine*, *388*(15), 1353–1364. https://doi.org/10.1056/NEJMoa2215024

Okendo, J., Koren, S., Rhie, A., Torrado-Tapias, A., Pickett, B. D., Brooks, S. Y., Bouffard, G. G., Crawford, J. K., Sison, C., Joardar, V. S., Murphy, T. D., Tierney, J. A. S., Haggerty, L., Martin, F. J., Wilson, C., Amores, A., Postlethwait, J. H., Murphy, J., Sakai, N., … Burgess, S. M. (2025). *Complete de novo assembly and re-annotation of the zebrafish genome* (p. 2025.11.17.688901). bioRxiv. https://doi.org/10.1101/2025.11.17.688901

Padilla, P. A., & Roth, M. B. (2001). Oxygen deprivation causes suspended animation in the zebrafish embryo. *Proceedings of the National Academy of Sciences of the United States of America*, *98*(13), 7331–7335. https://doi.org/10.1073/pnas.131213198

Parichatikanond, W., Luangmonkong, T., Mangmool, S., & Kurose, H. (2020). Therapeutic Targets for the Treatment of Cardiac Fibrosis and Cancer: Focusing on TGF-β Signaling. *Frontiers in Cardiovascular Medicine*, *7*. https://doi.org/10.3389/fcvm.2020.00034

Patel, Y., & Joseph, J. (2020). Sodium Intake and Heart Failure. *International Journal of Molecular Sciences*, *21*(24), 9474. https://doi.org/10.3390/ijms21249474

Pauwels, L., De Clercq, R., Goossens, J., Iñigo, S., Williams, C., Ron, M., Britt, A., & Goossens, A. (2018). A Dual sgRNA Approach for Functional Genomics in Arabidopsis thaliana. *G3: Genes|Genomes|Genetics*, *8*(8), 2603–2615. https://doi.org/10.1534/g3.118.200046

Pérez-Carrillo, L., Aragón-Herrera, A., Giménez-Escamilla, I., Delgado-Arija, M., García-Manzanares, M., Anido-Varela, L., Lago, F., Martínez-Dolz, L., Portolés, M., Tarazón, E., & Roselló-Lletí, E. (2022). Cardiac Sodium/Hydrogen Exchanger (NHE11) as a

Novel Potential Target for SGLT2i in Heart Failure: A Preliminary Study. *Pharmaceutics*, *14*(10), 1996. https://doi.org/10.3390/pharmaceutics14101996

Ponikowski, P., Voors, A. A., Anker, S. D., Bueno, H., Cleland, J. G. F., Coats, A. J. S., Falk, V., González-Juanatey, J. R., Harjola, V.-P., Jankowska, E. A., Jessup, M., Linde, C., Nihoyannopoulos, P., Parissis, J. T., Pieske, B., Riley, J. P., Rosano, G. M. C., Ruilope, L. M., Ruschitzka, F., … ESC Scientific Document Group. (2016). 2016 ESC Guidelines for the diagnosis and treatment of acute and chronic heart failure: The Task Force for the diagnosis and treatment of acute and chronic heart failure of the European Society of Cardiology (ESC)Developed with the special contribution of the Heart Failure Association (HFA) of the ESC. *European Heart Journal*, *37*(27), 2129–2200. https://doi.org/10.1093/eurheartj/ehw128

Pop-Busui, R., Januzzi, J. L., Bruemmer, D., Butalia, S., Green, J. B., Horton, W. B., Knight, C., Levi, M., Rasouli, N., & Richardson, C. R. (2022). Heart Failure: An Underappreciated Complication of Diabetes. A Consensus Report of the American Diabetes Association. *Diabetes Care*, *45*(7), 1670–1690. https://doi.org/10.2337/dci22-0014

Profire, B.-Ștefania, Lupașcu, F. G., Stătescu, C., Șorodoc, V., Sascău, R.-A., Profire, L., & Șorodoc, L. (2025). Heart Failure Biomarkers—Pathophysiology, Diagnosis, Prognosis and Clinical Relevance. *International Journal of Molecular Sciences*, *26*(19), 9740. https://doi.org/10.3390/ijms26199740

Rist, A., Sevre, K., Wachtell, K., Devereux, R. B., Aurigemma, G. P., Smiseth, O. A., Kjeldsen, S. E., Julius, S., Pitt, B., Burnier, M., Kreutz, R., Oparil, S., Mancia, G., & Zannad, F.

(2024). The current best drug treatment for hypertensive heart failure with preserved ejection fraction. *European Journal of Internal Medicine*, *120*, 3–10. https://doi.org/10.1016/j.ejim.2023.10.008

S., V., & Santhakumar, K. (2025). A pro-angiogenic and hypoxic zebrafish model as a novel platform for anti-angiogenic drug testing. *Biology Open*, *14*(8), bio061863. https://doi.org/10.1242/bio.061863

Safi, S., Korang, S. K., Nielsen, E. E., Sethi, N. J., Feinberg, J., Gluud, C., & Jakobsen, J. C. (2017). Beta-blockers for heart failure. *The Cochrane Database of Systematic Reviews*, *2017*(12), CD012897. https://doi.org/10.1002/14651858.CD012897

Sánchez-Iranzo, H., Galardi-Castilla, M., Sanz-Morejón, A., González-Rosa, J. M., Costa, R., Ernst, A., Sainz de Aja, J., Langa, X., & Mercader, N. (2018). Transient fibrosis resolves via fibroblast inactivation in the regenerating zebrafish heart. *Proceedings of the National Academy of Sciences of the United States of America*, *115*(16), 4188–4193. https://doi.org/10.1073/pnas.1716713115

Sayour, A. A., Ruppert, M., Oláh, A., Benke, K., Barta, B. A., Zsáry, E., Merkely, B., & Radovits, T. (2021). Effects of SGLT2 Inhibitors beyond Glycemic Control—Focus on Myocardial SGLT1. *International Journal of Molecular Sciences*, *22*(18), 9852. https://doi.org/10.3390/ijms22189852

Schafer, A. E. (2018). *The Role of MMP-13 in Cardiac Remodeling and Fibrosis* [University of Cincinnati]. https://etd.ohiolink.edu/acprod/odb_etd/etd/r/1501/10?clear=10&p10_accession_num=ucin1537949351943938

Schwinger, R. H. G. (2021). Pathophysiology of heart failure. *Cardiovascular Diagnosis and Therapy*, *11*(1), 26376–26276. https://doi.org/10.21037/cdt-20-302

Sethi, R., Jain, R., Raj, R. A., Pv, J., Arora, M., Thakran, V., Pandey, R. K., Sharma, J., Rao, K. M. M., Sharma, H., Francis, F., Sugumaran, A., & Mohanasundaram, S. (2026). Mineralocorticoid Receptor Antagonists: The Pillar Drug in Heart Failure. *Journal of The Association of Physicians of India*, *74*(1), 22–26. https://doi.org/10.59556/japi.74.1296

Shahim, B., Kapelios, C. J., Savarese, G., & Lund, L. H. (2023). Global Public Health Burden of Heart Failure: An Updated Review. *Cardiac Failure Review*, *9*, e11. https://doi.org/10.15420/cfr.2023.05

Shi, X., Verma, S., Yun, J., Brand-Arzamendi, K., Singh, K. K., Liu, X., Garg, A., Quan, A., & Wen, X.-Y. (2017). Effect of empagliflozin on cardiac biomarkers in a zebrafish model of heart failure: Clues to the EMPA-REG OUTCOME trial? *Molecular and Cellular Biochemistry*, *433*(1), 97–102. https://doi.org/10.1007/s11010-017-3018-9

Shohet, R. V., & Garcia, J. A. (2007). Keeping the engine primed: HIF factors as key regulators of cardiac metabolism and angiogenesis during ischemia. *Journal of Molecular Medicine*, *85*(12), 1309–1315. https://doi.org/10.1007/s00109-007-0279-x

Shrimpton, A. J., Walker, S. L. M., & Ackland, G. L. (2020). Angiotensin converting enzyme inhibitors and angiotensin receptor blockers. *BJA Education*, *20*(11), 362–367. https://doi.org/10.1016/j.bjae.2020.07.004

Sica, D. A. (2015). Mineralocorticoid Receptor Antagonists for Treatment of Hypertension and Heart Failure. *Methodist DeBakey Cardiovascular Journal*, *11*(4), 235–239. https://doi.org/10.14797/mdcj-11-4-235

Siddiqui, S., Siddiqui, H., Riguene, E., & Nomikos, M. (2025). Zebrafish: A Versatile and Powerful Model for Biomedical Research. *BioEssays*, *47*(12), e70080. https://doi.org/10.1002/bies.70080

Singleman, C., & Holtzman, N. G. (2012). Analysis of Post-Embryonic Heart Development and Maturation in the Zebrafish, Danio rerio. *Developmental Dynamics : An Official Publication of the American Association of Anatomists*, *241*(12), 1993–2004. https://doi.org/10.1002/dvdy.23882

Stead, L. F., Koilpillai, P., Fanshawe, T. R., & Lancaster, T. (2016). *Combined pharmacotherapy and behavioural interventions for smoking cessation—Stead, LF - 2016 | Cochrane Library*. https://www.cochranelibrary.com/cdsr/doi/10.1002/14651858.CD008286.pub3/full

Suissa, K., Larivière, J., Eisenberg, M. J., Eberg, M., Gore, G. C., Grad, R., Joseph, L., Reynier, P. M., & Filion, K. B. (2017). Efficacy and Safety of Smoking Cessation Interventions in Patients With Cardiovascular Disease. *Circulation: Cardiovascular Quality and Outcomes*, *10*(1), e002458. https://doi.org/10.1161/CIRCOUTCOMES.115.002458

Sur, A., Wang, Y., Capar, P., Margolin, G., Prochaska, M. K., & Farrell, J. A. (2023). Single-cell analysis of shared signatures and transcriptional diversity during zebrafish development. *Developmental Cell*, *58*(24), 3028-3047.e12. https://doi.org/10.1016/j.devcel.2023.11.001

Talha, K. M., Anker, S. D., & Butler, J. (2023). SGLT-2 Inhibitors in Heart Failure: A Review of Current Evidence. *International Journal of Heart Failure*, *5*(2), 82–90. https://doi.org/10.36628/ijhf.2022.0030

Taylor, C. T., & Scholz, C. C. (2022). The effect of HIF on metabolism and immunity. *Nature Reviews. Nephrology*, *18*(9), 573–587. https://doi.org/10.1038/s41581-022-00587-8

Teame, T., Zhang, Z., Ran, C., Zhang, H., Yang, Y., Ding, Q., Xie, M., Gao, C., Ye, Y., Duan, M., & Zhou, Z. (2019). The use of zebrafish (Danio rerio) as biomedical models. *Animal Frontiers: The Review Magazine of Animal Agriculture*, *9*(3), 68–77. https://doi.org/10.1093/af/vfz020

Travisano, S. I., & Lien, C.-L. (2025). Cardiac Regeneration and Repair in Zebrafish and Mammalian Models. *Current Cardiology Reports*, *27*(1), 95. https://doi.org/10.1007/s11886-025-02235-6

Umbrello, M., Dyson, A., Feelisch, M., & Singer, M. (2013). The Key Role of Nitric Oxide in Hypoxia: Hypoxic Vasodilation and Energy Supply–Demand Matching. *Antioxidants & Redox Signaling*, *19*(14), 1690–1710. https://doi.org/10.1089/ars.2012.4979

Vallon, V. (2024). State-of-the-Art-Review: Mechanisms of Action of SGLT2 Inhibitors and Clinical Implications. *American Journal of Hypertension*, *37*(11), 841–852. https://doi.org/10.1093/ajh/hpae092

Vallon, V., & Verma, S. (2021). Effects of SGLT2 Inhibitors on Kidney and Cardiovascular Function. *Annual Review of Physiology*, *83*(Volume 83, 2021), 503–528. https://doi.org/10.1146/annurev-physiol-031620-095920

Varshney, G. K., & Burgess, S. M. (2025). CRISPR-based functional genomics tools in vertebrate models. *Experimental & Molecular Medicine*, *57*(7), 1355–1372. https://doi.org/10.1038/s12276-025-01514-0

Vergani, M., Cannistraci, R., Perseghin, G., & Ciardullo, S. (2024). The Role of Natriuretic Peptides in the Management of Heart Failure with a Focus on the Patient with Diabetes. *Journal of Clinical Medicine*, *13*(20), 6225. https://doi.org/10.3390/jcm13206225

Verkerk, A. O., & Remme, C. A. (2012). Zebrafish: A novel research tool for cardiac (patho)electrophysiology and ion channel disorders. *Frontiers in Physiology*, *3*. https://doi.org/10.3389/fphys.2012.00255

Vornanen, M., & Hassinen, M. (2016). Zebrafish heart as a model for human cardiac electrophysiology. *Channels*, *10*(2), 101–110. https://doi.org/10.1080/19336950.2015.1121335

Warriner, D., Sheridan, P., & Lawford, P. (2015). Heart failure: Not a single organ disease but a multisystem syndrome. *British Journal of Hospital Medicine*, *76*(6), 330–336. https://doi.org/10.12968/hmed.2015.76.6.330

Weekes, A. J., Reddy, A., Lewis, M. R., & Norton, H. J. (2012). E-Point Septal Separation Compared to Fractional Shortening Measurements of Systolic Function in Emergency Department Patients: Prospective Randomized Study. *Journal of Ultrasound in Medicine*, *31*(12), 1891–1897. https://doi.org/10.7863/jum.2012.31.12.1891

Wei, X., Hou, Y., Long, M., Jiang, L., & Du, Y. (2022). Molecular mechanisms underlying the role of hypoxia-inducible factor-1 α in metabolic reprogramming in renal fibrosis. *Frontiers in Endocrinology*, *13*. https://doi.org/10.3389/fendo.2022.927329

Weinberger, M., Simões, F. C., Gungoosingh, T., Sauka-Spengler, T., & Riley, P. R. (2024). Distinct epicardial gene regulatory programs drive development and regeneration of the zebrafish heart. *Developmental Cell*, *59*(3), 351-367.e6. https://doi.org/10.1016/j.devcel.2023.12.012

Wijerathna, H. M. S. M., Shanaka, K. A. S. N., Raguvaran, S. S., Jayamali, B. P. M. V., Kim, S.-H., Kim, M.-J., Jung, S., & Lee, J. (2024). CRISPR/Cas9-Mediated fech Knockout Zebrafish: Unraveling the Pathogenesis of Erythropoietic Protoporphyria and Facilitating Drug Screening. *International Journal of Molecular Sciences*, *25*(19), 10819. https://doi.org/10.3390/ijms251910819

Xia, Y., Duca, S., Perder, B., Dündar, F., Zumbo, P., Qiu, M., Yao, J., Cao, Y., Harrison, M. R. M., Zangi, L., Betel, D., & Cao, J. (2022). Activation of a transient progenitor state in the epicardium is required for zebrafish heart regeneration. *Nature Communications*, *13*(1), 7704. https://doi.org/10.1038/s41467-022-35433-9

Xu, S., Liu, C., Xie, F., Tian, L., Manno, S. Hc., Manno, F. A. M., Fallah, S., Pelster, B., Tse, G., & Cheng, S. H. (2019). Excessive inflammation impairs heart regeneration in zebrafish breakdance mutant after cryoinjury. *Fish & Shellfish Immunology*, *89*, 117–126. https://doi.org/10.1016/j.fsi.2019.03.058

Xu, S., Webb, S. E., Lau, T. C. K., & Cheng, S. H. (2018). Matrix metalloproteinases (MMPs) mediate leukocyte recruitment during the inflammatory phase of zebrafish heart

regeneration. *Scientific Reports*, *8*(1), 7199. https://doi.org/10.1038/s41598-018-25490-w

Yoshikawa, H., Suzuki, M., Hashimoto, G., Kusunose, Y., Otsuka, T., Nakamura, M., & Sugi, K. (2012). Midwall ejection fraction for assessing systolic performance of the hypertrophic left ventricle. *Cardiovascular Ultrasound*, *10*(1), 45. https://doi.org/10.1186/1476-7120-10-45

Zannad, F., Gattis Stough, W., Rossignol, P., Bauersachs, J., McMurray, J. J. V., Swedberg, K., Struthers, A. D., Voors, A. A., Ruilope, L. M., Bakris, G. L., O'Connor, C. M., Gheorghiade, M., Mentz, R. J., Cohen-Solal, A., Maggioni, A. P., Beygui, F., Filippatos, G. S., Massy, Z. A., Pathak, A., … Pitt, B. (2012). Mineralocorticoid receptor antagonists for heart failure with reduced ejection fraction: Integrating evidence into clinical practice. *European Heart Journal*, *33*(22), 2782–2795. https://doi.org/10.1093/eurheartj/ehs257

Zhang, M., & Shah, A. M. (2020). Nitric oxide fine-tunes NHE1 to control cardiomyocyte pH. *Cardiovascular Research*, *116*(12), 1925–1926. https://doi.org/10.1093/cvr/cvaa065

Zhang, S., Liu, C., Zhang, Y., Wu, Z., Feng, K., Lai, Y., Pei, J., & Guan, T. (2023). Different heart failure phenotypes of valvular heart disease: The role of mitochondrial dysfunction. *Frontiers in Cardiovascular Medicine*, *10*, 1135938. https://doi.org/10.3389/fcvm.2023.1135938

Zhang, Y., Bao, Y.-C., Wang, L.-X., Zhao, H.-J., Sun, J., Sun, L., Duan, W., Du, M., Wang, L.-J., An, Q.-Y., & Yang, W.-Z. (2025). Mineralocorticoid receptor antagonists in heart

failure: A systematic review and meta-analysis. *Frontiers in Cardiovascular Medicine*, *12*, 1667236. https://doi.org/10.3389/fcvm.2025.1667236

Zhao, M., Li, N., & Zhou, H. (2023). SGLT1: A Potential Drug Target for Cardiovascular Disease. *Drug Design, Development and Therapy*, *17*, 2011–2023. https://doi.org/10.2147/DDDT.S418321

Zhao, Y., Yun, M., Nguyen, S. A., Tran, M., & Nguyen, T. P. (2019). In Vivo Surface Electrocardiography for Adult Zebrafish. *Journal of Visualized Experiments : JoVE*, (150), 10.3791/60011. https://doi.org/10.3791/60011

Zhou, L., Cryan, E. V., D'Andrea, M. R., Belkowski, S., Conway, B. R., & Demarest, K. T. (2003). Human cardiomyocytes express high level of Na+/glucose cotransporter 1 (SGLT1). *Journal of Cellular Biochemistry*, *90*(2), 339–346. https://doi.org/10.1002/jcb.10631

Zhu, C., Cheng, M., Su, Y., Ma, T., Lei, X., & Hou, Y. (2022). Effect of Dietary Sodium Restriction on the Quality of Life of Patients With Heart Failure: A Systematic Review of Randomized Controlled Trials. *Journal of Cardiovascular Nursing*, *37*(6), 570. https://doi.org/10.1097/JCN.0000000000000880

Zhu, Y., Lv, C., Yang, H., Lu, Q., Wang, X., Zhang, Y., Guo, M., & Yang, B. (2025). Chronic cardiorenal syndrome: Cardio-renal protective effect of SGLT2i. *Renal Failure*, *47*(1), 2575921. https://doi.org/10.1080/0886022X.2025.2575921

Zuchi, C., Tritto, I., Carluccio, E., Mattei, C., Cattadori, G., & Ambrosio, G. (2020). Role of endothelial dysfunction in heart failure. *Heart Failure Reviews*, *25*(1), 21–30. https://doi.org/10.1007/s10741-019-09881-3

7. Supplementary material

Supplementary Table 1. Raw fractional shortening (FS%) values for all experimental groups at baseline

Neg. Ctrl	*slc5a1*	*slc5a2*	*mmp13a*	*mmp13b*
16.78	14.22	14.67	15.62	16.74
18.83	18.96	9.86	21.44	17.82
11.46	21.24	19.20	12.05	17.38
12.96	13.43	14.73	23.63	14.58
16.97	10.33	10.18	12.7	7.84
19.71	13.31	12.15	22.9	11.01
13.33	19.46	13.93	0.0	15.84
9.85	12.68	29.31	45.4	
21.97	15.78	21.42	23.2	
16.81		19.14	4.7	
14.15		22.69	0.0	
20.66		25.34	18.7	
10.42		12.46	12.7	
15.80		26.97	9.2	
13.77		14.59	0.0	
11.27			0.0	
19.65				
26.16				
14.9				
16.84				
14.19				
16.08				
17.76				
17.00				
12.48				

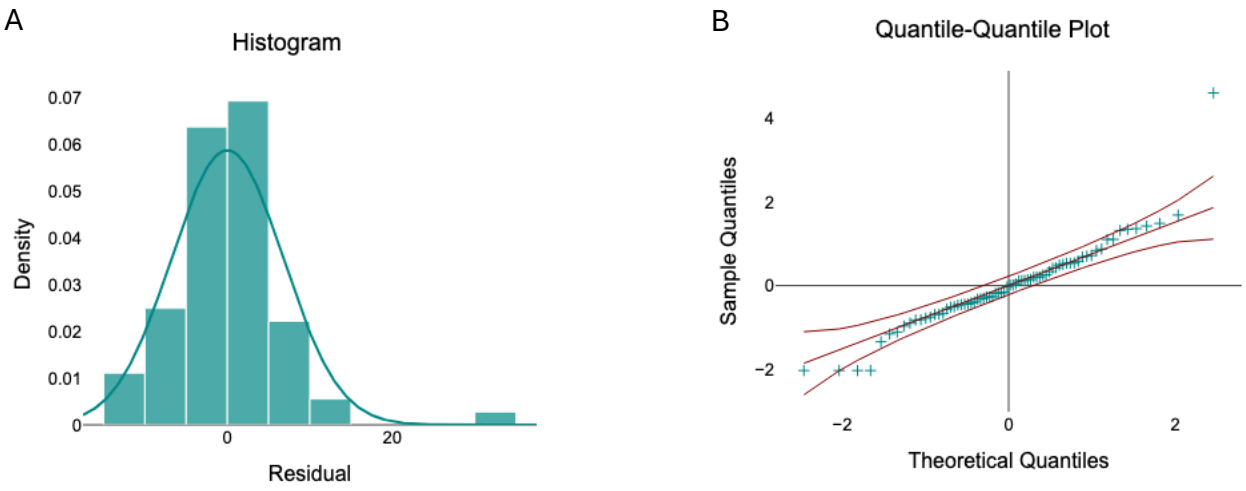

Supplementary Figure 1. *Histogram (A) and Q-Q plot (B) of ANOVA model residuals for fractional shortening (FS%) data at baseline. The histogram displays the distribution of residuals with a normal distribution curve. The Q-Q plot compares sample quantiles against theoretical quantiles, with red lines indicating 95% confidence bands. Visual inspection indicates approximate normality of residuals across all groups.*

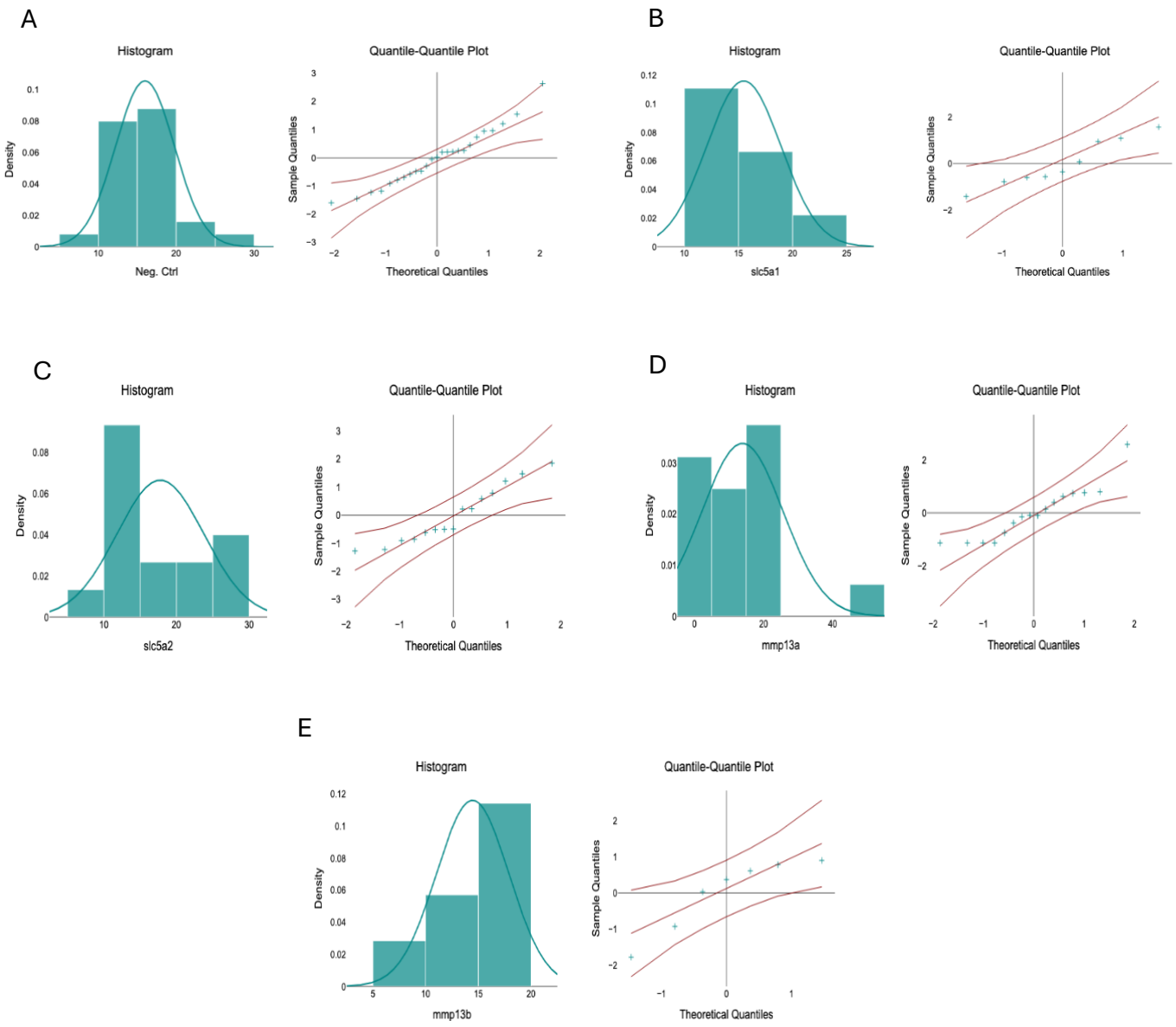

Supplementary Figure 2. *Histogram and Q-Q plot of fractional shortening (FS%) for each experimental group. Graphs are shown for (A) Negative Control, (B) slc5a1, (C) slc5a2, (D) mmp13a, and (E) mmp13b knockouts. Each histogram displays data distribution with a normal curve, and Q-Q plots show alignment with theoretical quantiles, indicating normality within each group.*

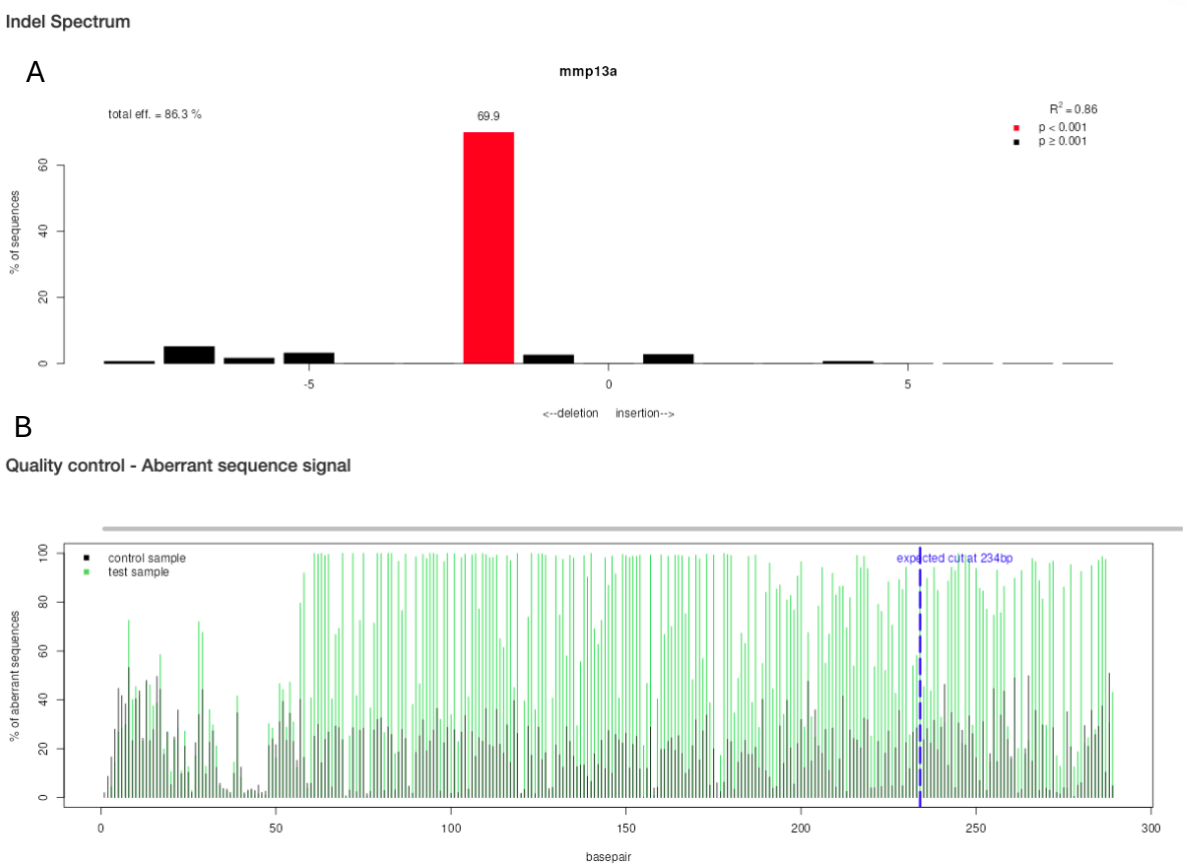

Supplementary Figure 3. *TIDE analysis of CRISPR/Cas9 editing efficiency for mmp13a. (A) Indel spectrum showing a total editing efficiency of 86.3% (R^2 = 0.86), with a predominant -1 deletion (69.9%, p < 0.001) at the expected cut site. (B) Quality control plot showing aberrant sequence signal in control (black) and CRISPR/Cas9 knockout sample (green), with the expected cut site at 234 bp (blue dotted line).*

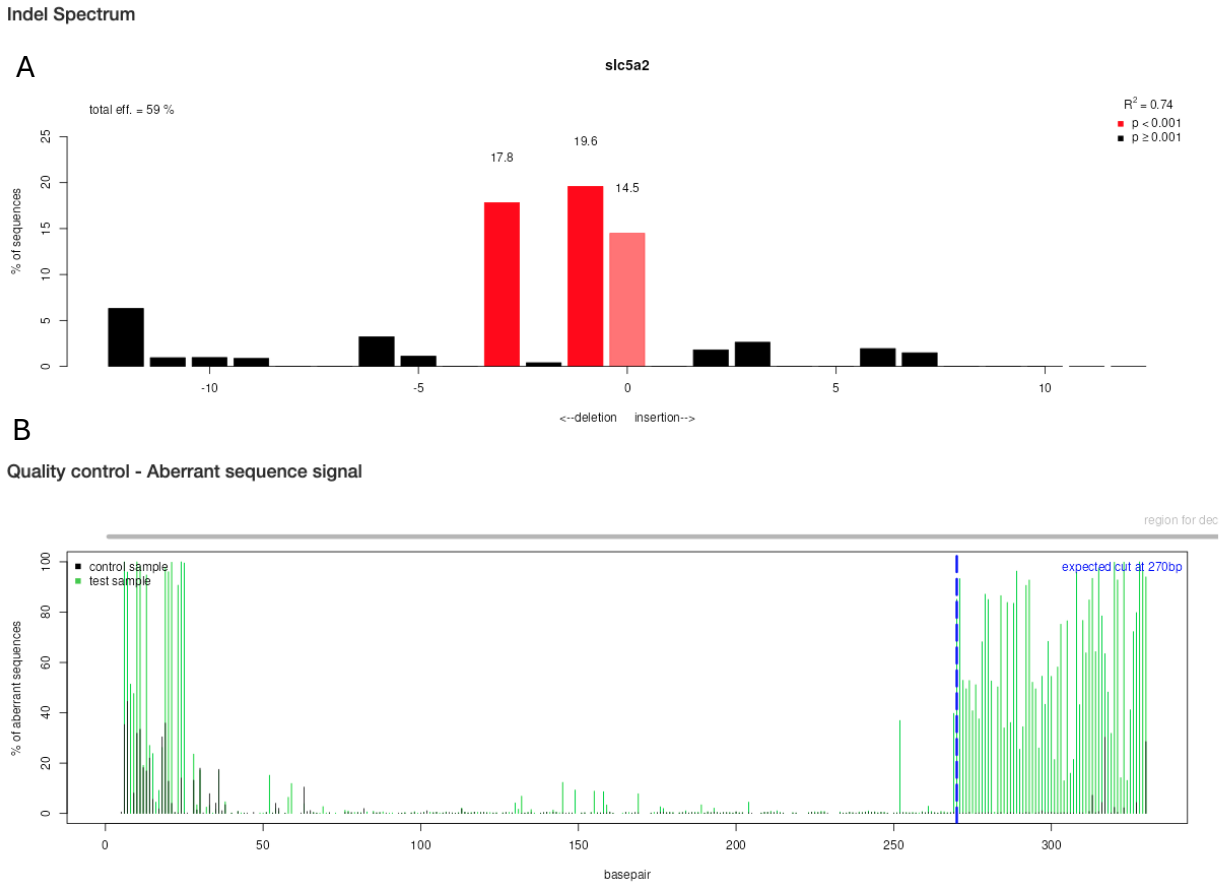

Supplementary Figure 4. *TIDE analysis of CRISPR/Cas9 editing efficiency for slc5a2. (A) Indel spectrum showing a total editing efficiency of 59% (R^2 = 0.74), with predominant mutations of -1 deletion (19.6%). (B) Quality control plot showing aberrant sequence signal in the control (black) and CRISPR/Cas9 knockout sample (green), with the expected cut site at 270 bp (blue dotted line)*

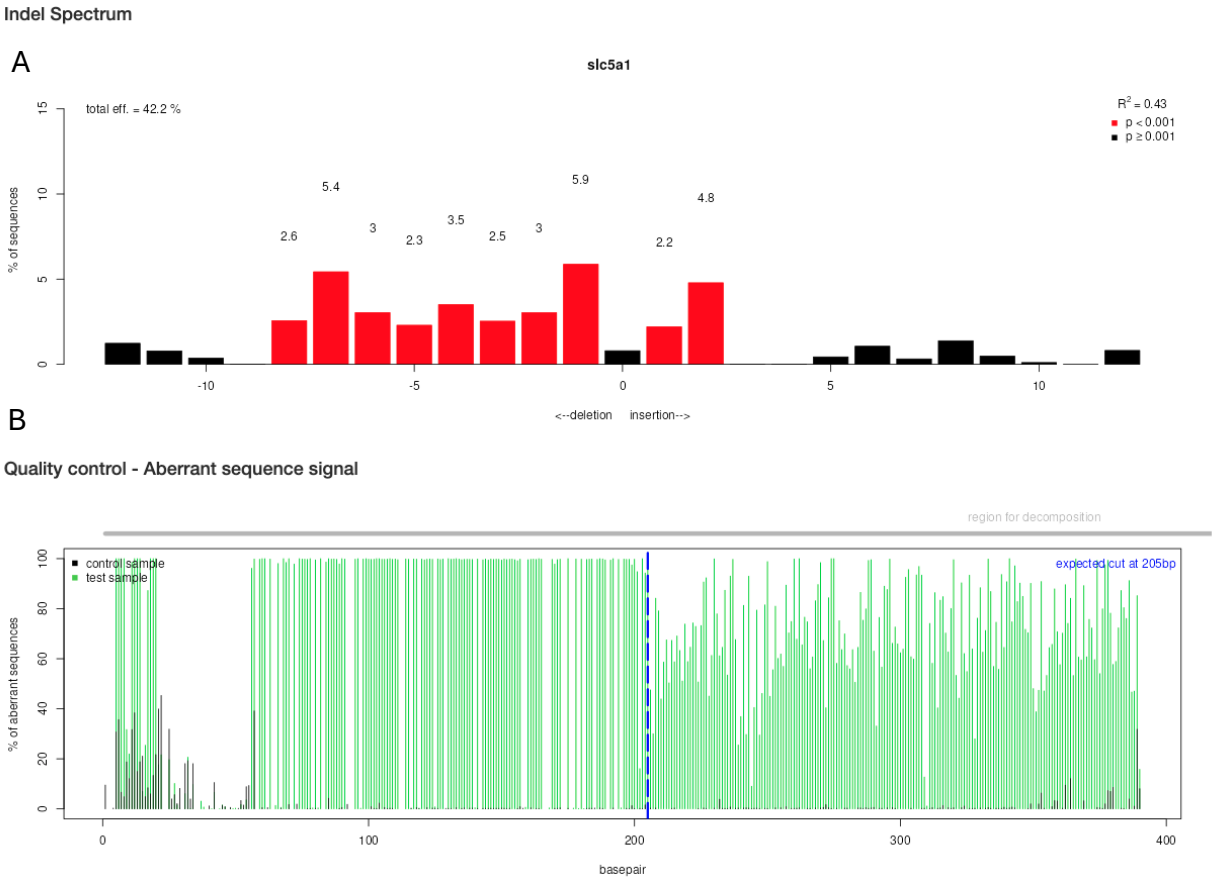

Supplementary Figure 5. TIDE *analysis of CRISPR/Cas9 editing efficiency for slc5a1. (A) Indel spectrum showing a total editing efficiency of 42.2% (R^2 = 0.43), with multiple significant indels distributed across sizes at the expected cut site. (B) Quality control plot showing aberrant sequence signal in the control (black) and CRISPR/Cas9 knockout sample (green), with the expected cut site at 205 bp (blue dotted line)*

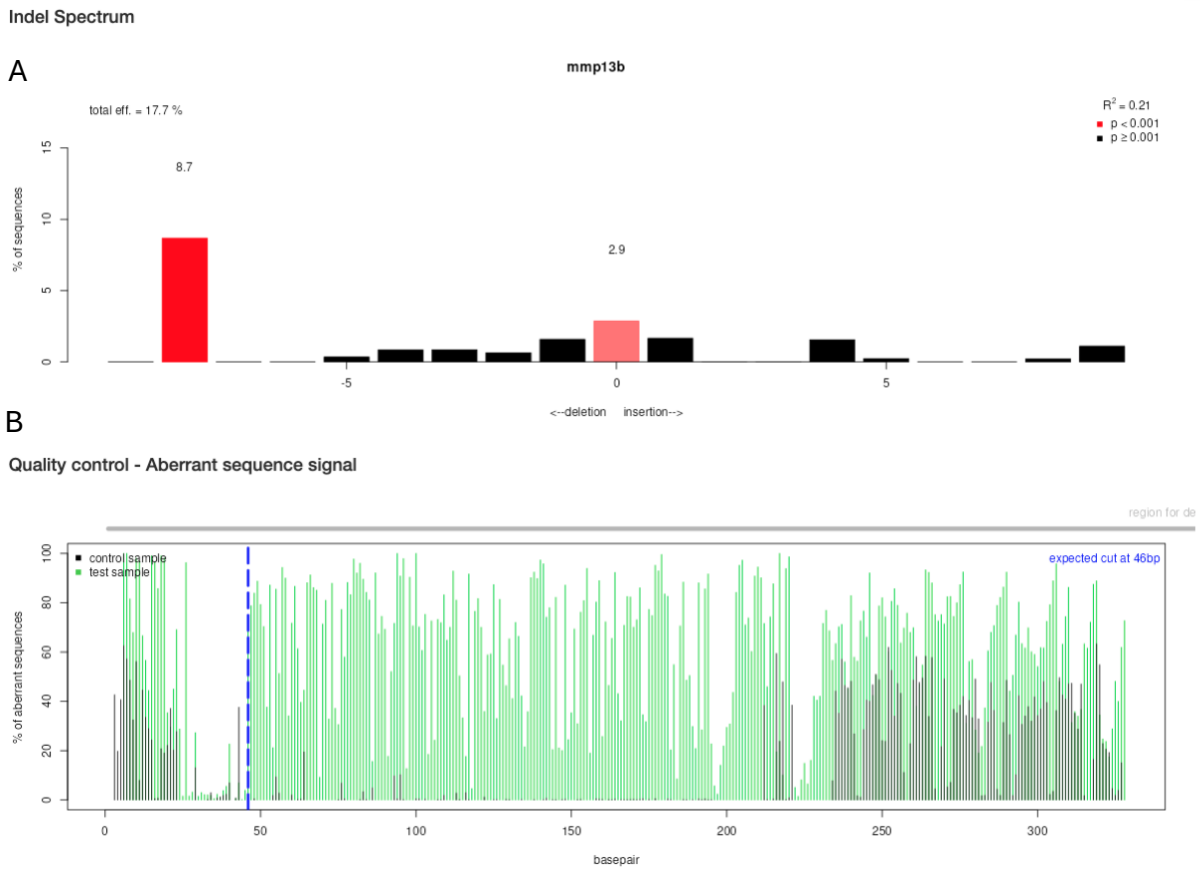

Supplementary Figure 6. *TIDE analysis of CRISPR/Cas9 editing efficiency for mmp13b. (A) Indel spectrum showing a total editing efficiency of 17.7% (R^2 = 0.21), with a predominant -8 deletion (8.7%) at the expected cut site. (B) Quality control plot showing aberrant sequence signal in the control (black) and CRISPR/Cas9 knockout sample (green), with the expected cut site at 46 bp (blue dotted line)*

Supplementary Table 2. Raw fractional shortening (FS%) values for all experimental groups after 45 minutes of hypoxia exposure

Neg. Ctrl	***slc5a1***	***slc5a2***	***mmp13a***	***mmp13b***
10.92	15.58	28.15	20.92	11.55
22.47	20.85	26.35	16.22	13.31
27.68	21.82	21.70	15.59	19.91
22.52	23.48	23.79	24.15	24.04
28.39	26.00	27.76	14.54	15.59
29.46	23.20	22.62	12.73	13.08
20.39	18.21	21.36	18.22	14.61
19.17	19.16	20.75	27.37	8.44
26.26	24.30	23.49		14.40
19.34	22.88	27.80		17.05
20.22	24.82	29.76		
26.65	31.83	18.65		
15.95	28.91	17.24		
16.55	21.48	22.92		
20.67	21.39	26.03		
17.59	25.17			
9.84	23.04			
17.76	20.92			
	22.49			
	25.97			
	21.68			
	23.37			

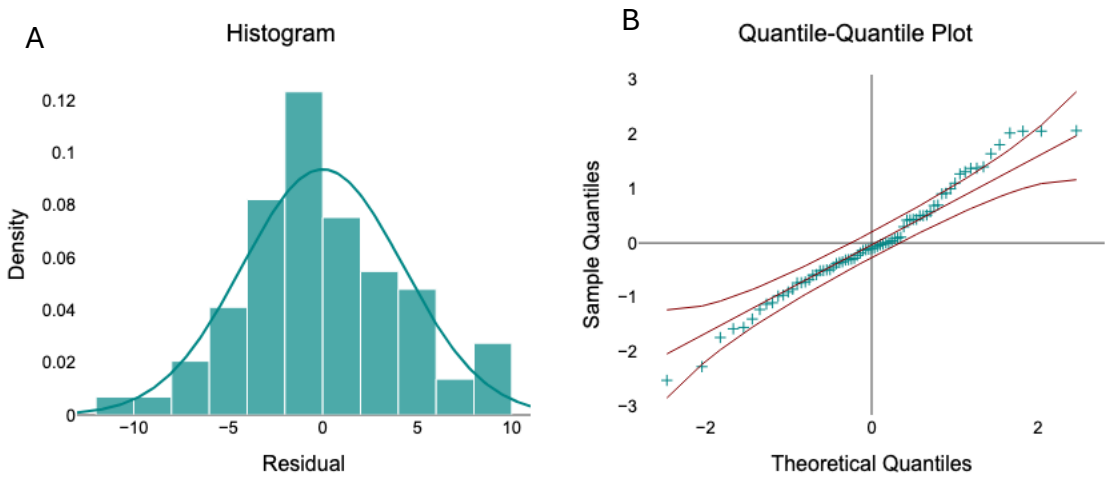

Supplementary Figure 7. *Histogram (A) and Q-Q plot (B) of ANOVA model residuals for fractional shortening (FS%) following 45 minutes of hypoxia exposure at 3 dpf. The histogram displays the distribution of residuals with a normal distribution curve.*

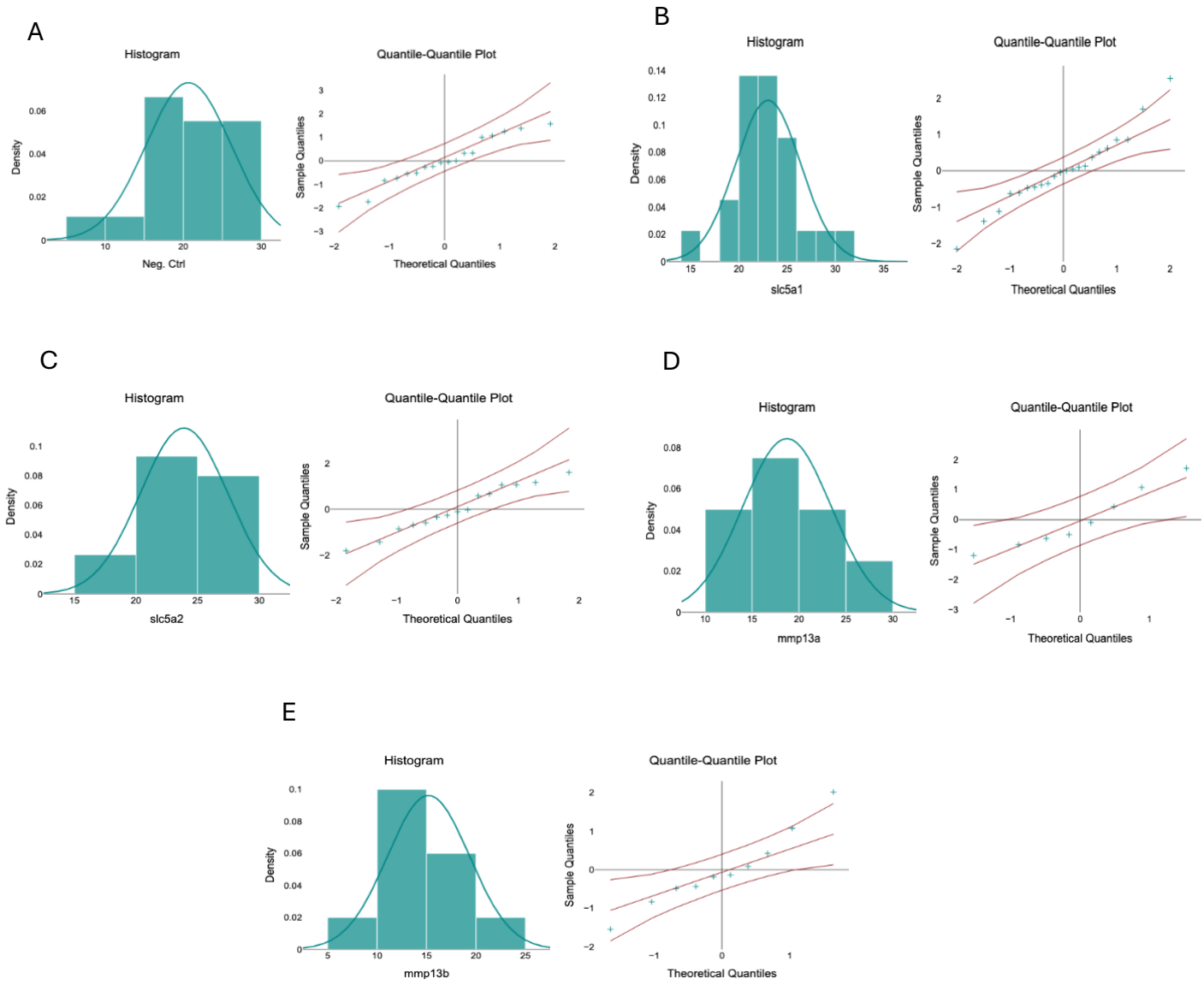

Supplementary Figure 8. *Individual histograms and Q-Q plots of fractional shortening (FS%) following 45 minutes of hypoxia exposure at 3 dpf for Neg. Ctrl (A), slc5a1 (B), slc5a2 (C), mmp13a (D), and mmp13b (E). Each histogram displays data distribution with a normal curve, and Q-Q plots show alignment with theoretical quantiles, supporting normality within each group.*

Supplementary Table 3. Raw fractional shortening (FS%) values for all experimental groups after 60 minutes of hypoxia exposure

Neg_ctrl_normoxia	Neg_ctrl_hypoxia	*slc5a1*	*slc5a2*
14.25	19.84	19.84	19.61
15.48	8.18	15.94	16.67
17.76	15.33	24.54	16.63
13.88	16.37	18.03	16.15
17.75	10.27	22.43	11.86
12.13	10.83	13.06	16.88
12.62	15.80	19.16	23.66
15.75	15.91	17.39	20.00
22.82	10.32	23.27	18.98
20.06	12.71	12.18	16.91
20.40	16.04	15.06	20.97
17.27	17.11	18.89	14.52
17.76	18.38	20.06	23.65
12.28	20.35	27.28	14.60
13.08	17.71	15.77	18.80
19.65	10.62	29.35	16.92
22.85	20.04	13.99	12.39
19.08	18.66	19.85	18.83
23.62	16.10	23.51	16.92
14.80	8.56	19.20	25.74
17.57	18.40	23.75	20.66
20.12	13.36	27.67	15.69
20.50	11.07	17.18	19.78
15.16	11.49	15.23	25.05
13.76	17.88	20.88	27.98
18.89	9.83	14.21	15.26
17.54	16.73	16.36	19.70
23.08	14.92	15.85	
18.59	23.73	13.41	
18.61	15.63	18.55	
17.61	9.34	20.66	
20.05	12.86		
18.63	12.83		
17.05	33.59		
16.92	12.78		
20.38	13.98		
12.18	13.74		
23.16	21.24		

24.49	13.86		
18.95	14.00		
15.42	16.52		
18.33	16.65		
	13.25		

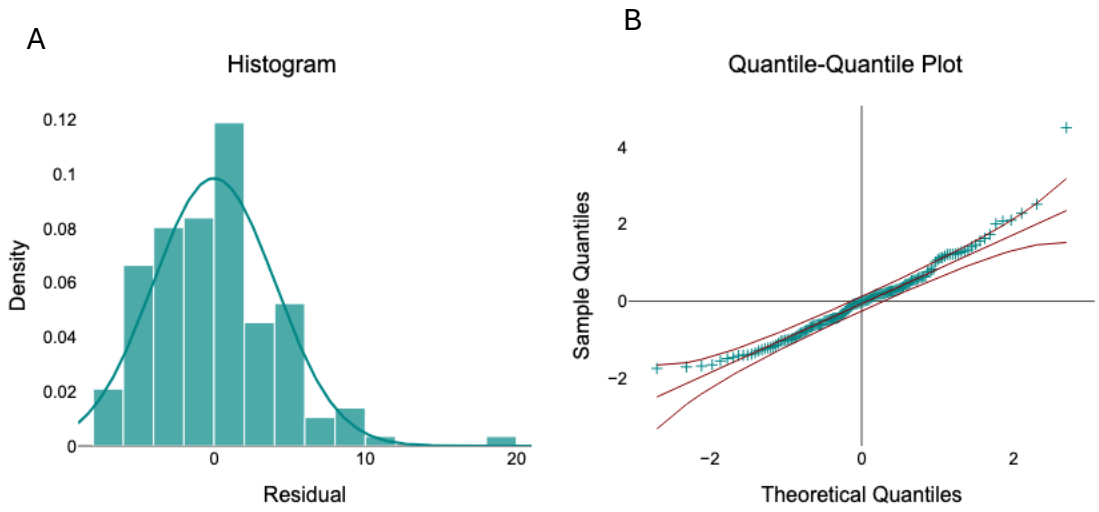

Supplementary Figure 9. *Histogram (A) and Q-Q plot (B) of ANOVA model residuals for fractional shortening (FS%) following 60 minutes of hypoxia exposure at 3 dpf.*

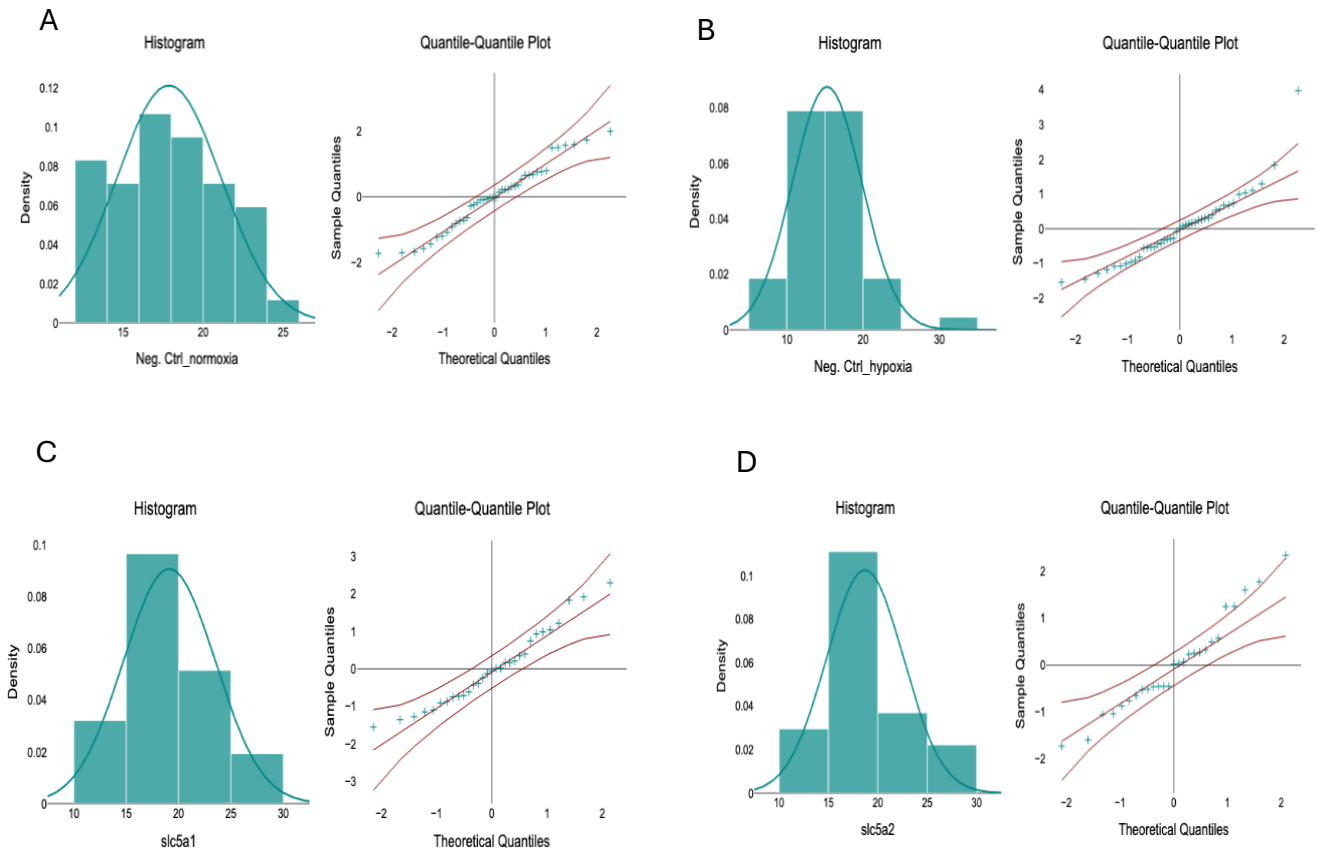

Supplementary Figure 10. *Individual histograms and Q-Q plots of fractional shortening (FS%) following 60 minutes of hypoxia exposure at 3 dpf for Neg. Ctrl_normoxia (A), Neg. Ctrl_hypoxia (B), slc5a1 (C), and slc5a2 (D).*

8. Appendix A

QuillBot was used as a plugin with Microsoft Word as a supportive tool in correcting the English language (e.g., spelling/grammar checking and text-editing assistance) to improve clarity, readability, and consistency in the text.